Engineering Structures 56 (2013) 1164–1176

Contents lists available at SciVerse ScienceDirect

Engineering Structures

journal homepage: www.elsevier.com/locate/engstruct

A composite beam finite element for multibody dynamics: Application to large wind turbine modeling

C. Martín Saravia *, Sebastián P. Machado, Víctor H. Cortínez

Centro de Investigación en Mecánica Teórica y Aplicada, CONICET-Universidad Tecnológica Nacional, Facultad Regional Bahía Blanca, 11 de Abril 461, 8000 Bahía Blanca, Argentina

ARTICLE INFO

Article history:
Received 15 November 2012
Accepted 17 June 2013
Available online 27 July 2013

Keywords:
Wind turbines
Total Lagrangian
Anisotropic materials
Multibody systems

ABSTRACT

This work presents a beam finite element with multibody capabilities for modeling high aspect ratio composite wind turbine components, particularly the tower and the blades. The proposed formulation is based on an Updated Lagrangian approach, in which the virtual work equations are written as a function the director field and its derivatives. The cross-sectional modeling of the wind turbine components is based on the constitutive relations obtained from the analysis of the mechanics of composite laminates. The formulation of the equations of motion and the derivation of a hinge joint is presented. Several results for a large wind turbine model are shown.

1. Introduction

The extraction of energy from the wind is one of the main topics of research in the engineering community. Particularly, the use of horizontal axis turbines is one of the most efficient methods to extract this energy and the fact that the extracted power mostly depends on the turbine rotor diameter is continuously pushing the geometric limit of the designs. Today the largest wind turbine in the world equipped with 64 m blades but it is expected in the near future that prototypes of wind turbines with 100 m blades appear. A question naturally arises about how affective are the available engineering tools to study these new designs. Many discussions have been made about the end of the geometrically linear theories era in the wind turbine structural modeling scenario, but the open question prevails: how effective structural linear theories are to predict the behavior of modern wind turbines within an acceptable precision?

The dynamic behavior of large wind turbines is frequently analyzed by means of flexible multibody systems and blades modeling is frequently done with thin-walled beam theory. The analysis of very flexible multibody beams involves a deep knowledge of tridimensional finite rotations. The nonvectorial nature of finite rotations introduces a great complexity to the finite element formulation. Several approaches have been proposed in the literature to address this problem, but the most powerful is based on the concept of the geometrically exact beam finite element, which can be traced back to the works of Simo [1] and Cardona [2]. After these pioneering works, other authors have addressed the problem of geometrically exact beams [3–12]. For its capability to deal with composite material, particularly useful in the present context are the geometrically exact Eulerian and Total Lagrangian formulations presented by Saravia et al. [11,13].

The cross-sectional stiffness that feeds the beam theory can be by three different methods; 3D finite element analysis, 2D finite element analysis and Classical Lamination Theory (CLT). 3D finite element approaches are very effective and could be considered the most accurate. The methods based on 2D finite element model of the cross-section are mainly due to Hodges et al. [14–17]; they has been frequently used in the analysis of composite blades and results to be very effective. The CLT approaches generally rely on the construction of an analytical function of the cross-section which is then integrated to obtain the stiffness parameters [18]. They are very fast and simple and if used carefully they can give excellent results.

Regarding multibody modeling of wind turbines, generally beam finite element formulations are used because of its capability to accurately predict the structural behavior of both the tower and the blades, also accounting for the interaction phenomena between them. The development of finite element algorithms for flexible multibody applications started in the early nineties with the work of Cardona et al. [19]. New approaches were quickly developed [20,21] and the different successful implementations pushed the subject from the scientific to the technological level. Most of the multibody beam formulations were developed using an isotropic constitutive law, although its capability to be fed with stiffness matrices of composite cross-sections is retained. A few ad hoc geometrically exact composite thin-walled beam formulations for multibody applications have been reported in the literature. Most of the formulations are based on the VAM (Variational Asymptotic

* Corresponding author. Tel.: +54 2914555220.
E-mail address: msaravia@conicet.gov.ar (C.M. Saravia).

0141-0296/$ - see front matter © 2013 Elsevier Ltd. All rights reserved.
http://dx.doi.org/10.1016/j.engstruct.2013.06.037

Method) approach [14–17] were developed for helicopter rotor modeling and were successfully applied to wind turbines in the last years [22]. The theory is very effective and accurate, but it requires a 2D finite element discretization of the cross-section in order to obtain the cross-sectional stiffness.

It is also common to find wind turbine analyzes that use an isotropic constitutive law [18,23–26], however this constitutive law is not capable of accurately describing the real behavior modern wind turbine blades, because they are built of highly heterogeneous sections made of composite materials. Also, many of the flexible multibody formulations used for modeling wind turbine blades assume linearity of the kinematic variables with respect to some intermediate frame of reference [18,23,27–29]. Of course this assumption introduces uncertainty, especially in the case of the highly flexible modern wind turbine designs.

Geometrically nonlinear modeling of wind turbines is not an extensively used approach [18]; although, it is possible to find several studies about the dynamic behavior of wind turbines using commercial software that provides geometrically nonlinear finite element formulations [30]. Nonlinear aeroelastic simulation of tilt-rotors using multibody procedures was done in [31] using the nonlinear finite element formulation described in [32]. Also, aero-servo-elastic modeling and control of wind turbines using finite-element multibody procedures was done in [33]. Other interesting works regarding the influence of geometrical nonlinearities in the dynamic behavior of wind turbines can be found in [27,34–36].

According to the stated situation about the wind turbine modeling trends, we propose in this work a composite beam multibody formulation that can contribute to the study of the nonlinear dynamic behavior of these machines. The static part of the present formulation is based on the adaptation of the previous developed geometrically exact composite beam finite element formulation [13] to an Updated Lagrangian approach; this is done to avoid the singularities of the rotation tensor. The resulting approach is frame invariant and thus capable of describing the deformation state of a multibody system. In contrast to the developments in [13], the present formulation can deal with the dynamic problem. This extension in the modeling capability is based on the introduction of the key concepts of the dynamic of flexible multibodies; (i) the treatment of arbitrary rotations, (ii) the development of the equations of joints and (iii) the development of the inertial virtual work. The treatment of arbitrary rotations is aided by the use of an Updated Lagrangian approach based on spatial nodal directors; the singularities of the rotation manifold are avoided by updating the reference rotation periodically and the director field is used to evaluate the deformation state of the bodies without being updated.

Also, a novel aspect of the present formulation is the development of a viscous joint. This joint is formulated based on the dynamic relations between the director vectors of master and slave nodes; thus, the dissipative effect of the joint can model the wind turbine generator torque. The main advantages of modeling the generator torque as a viscous joint are the avoidance of tracking the orientation of the generator shaft and the elimination of the complexities due to the work conjugacy of applied moments.

Results of the application of the present formulation to the analysis of a modern large scale wind turbine are presented; this includes several plots showing the temporal evolution of the most important variables of the wind turbine multibody model

2. Beam theory

2.1. Kinematics

The kinematic description of the thin-walled beam relates two states of a beam, an undeformed reference state $\mathcal{B}_0$, and a deformed state $\mathcal{B}$. We associate to $\mathcal{B}_0$ a material frame $\boldsymbol{E}_i$ and to $\mathcal{B}$ a spatial (floating) frame $\boldsymbol{e}_i$, both frames being orthonormal and coincident at time $t = 0$. The absolute displacements that occur during finite deformation are measured by a vector $\boldsymbol{u} = (u_1, u_2, u_3)$. The relation between the orthonormal frames is given by the linear transformation:

$$\boldsymbol{e}_i = \boldsymbol{\Lambda}(\boldsymbol{\theta}(x,t))\boldsymbol{E}_i, \tag{1}$$

where $\boldsymbol{\Lambda}(\boldsymbol{\theta}(x,t))$ is the total rotation tensor (a two-point tensor field $\in$SO(3); the special orthogonal Lie group) and $\boldsymbol{\theta}$ is the total Cartesian rotation vector.

Using Eq. (1) we can write the position vectors of a point in the beam in the reference and current configuration respectively as:

$$\begin{aligned}\boldsymbol{X}(x,\xi_2,\xi_3) &= \boldsymbol{X}_0(x) + \sum_{i=2}^{3}\xi_i\boldsymbol{E}_i,\\ \boldsymbol{x}(x,\xi_2,\xi_3,t) &= \boldsymbol{x}_0(x,t) + \sum_{i=2}^{3}\xi_i\boldsymbol{e}_i.\end{aligned} \tag{2}$$

In these equations the first term stands for the position a reference point and the second term stands for the position a point in the cross-section relative to the reference point. In this work we set the centroid to be the reference point. We can also express the spatial position vector as:

$$\boldsymbol{x}(x,\xi_2,\xi_3,t) = \boldsymbol{x}_0(x,t) + \boldsymbol{\Lambda}(x,t)\boldsymbol{\xi}, \tag{3}$$

where $\boldsymbol{\xi} = \sum_{i=2}^{3}\xi_i\boldsymbol{E}_i$ is the material position vector of a point with respect to the centroid. Note that, x is the running length coordinate and ξ_2 and ξ_3 are cross-section coordinates. Also, the displacement field is:

$$\boldsymbol{u}(x,\xi_2,\xi_3,t) = \boldsymbol{x} - \boldsymbol{X} = \boldsymbol{u}_0(x,t) + (\boldsymbol{\Lambda}(x,t) - \boldsymbol{I})\sum_{2}^{3}\xi_i\boldsymbol{E}_i, \tag{4}$$

where $\boldsymbol{u}_0$ represents the displacement of the centroid. The nonlinear manifold of 3D rotation transformations $\boldsymbol{\Lambda}$ (belonging to the special orthogonal Lie Group SO(3)) is obtained mathematically by means of a trigonometric form in terms of the Cartesian rotation vector $\boldsymbol{\theta}$ [2,37]. The set of kinematic variables is defined by three displacements and three increments of the rotational vector $\boldsymbol{\theta}$ as:

$$\begin{aligned}\mathcal{V} :=\ & \{\boldsymbol{\phi} = [\boldsymbol{u}_0,\boldsymbol{\theta}]^T : [0,\ell] \to R^3\}, [\boldsymbol{u}_0,\boldsymbol{\theta}]^T\\ =\ & [u_{01},u_{02},u_{03},\theta_1,\theta_2,\theta_3]^T.\end{aligned} \tag{5}$$

Note that although we have designed the rotational kinematic variable as the incremental rotation vector with respect to the previous converged configuration, the development of virtual quantities is almost identical to that of a formulation parametrized with the total rotation vector. For the sake of simplicity in the notation, we will develop the virtual quantities of the formulation naming $\boldsymbol{\theta}$ as the *rotation vector*, without specifying if it is an incremental or total quantity. In the finite element implementation we shall introduce the key aspects of the Updated Lagrangian Approach and clearly distinguish between total and incremental rotations.

2.2. Strains

In order to obtain the expression of the Green-Lagrange strains we first obtain the derivatives of the position vectors of the undeformed and deformed configurations as:

$$\begin{aligned}&\boldsymbol{X}_{,1} = \boldsymbol{X}_0' + \xi_2\boldsymbol{E}_2' + \xi_3\boldsymbol{E}_3', \quad \boldsymbol{X}_{,2} = \boldsymbol{E}_2, \quad \boldsymbol{X}_{,3} = \boldsymbol{E}_3,\\ &\boldsymbol{x}_{,1} = \boldsymbol{x}_0' + \xi_2\boldsymbol{e}_2' + \xi_3\boldsymbol{e}_3', \quad \boldsymbol{x}_{,2} = \boldsymbol{e}_2, \quad \boldsymbol{x}_{,3} = \boldsymbol{e}_3,\end{aligned} \tag{6}$$

where the subindex, i indicates derivative with respect to the ith coordinate. Injecting these vectors into the GL strain $\boldsymbol{E}_{GL} = \frac{1}{2}(\boldsymbol{x}_{,i}\cdot\boldsymbol{x}_{,j} - \boldsymbol{X}_{,i}\cdot\boldsymbol{X}_{,j})$ [38] we obtain three nonvanishing compo-

nents; in vector notation: $\boldsymbol{E}_{GL} = [E_{11}\, 2E_{12}\, 2E_{13}]^T$. Note that the existence of transverse shear strains implies $\boldsymbol{e}_1 \cdot \boldsymbol{x}_{,1} \neq 0$.

We can write the GL strain as:

$$\boldsymbol{E}_{GL} = \boldsymbol{D}\ \boldsymbol{\varepsilon}, \tag{7}$$

where we have introduced a generalized strain vector such that:

$$\boldsymbol{D} = \begin{bmatrix} 1 & \xi_3 & \xi_2 & 0 & 0 & 0 & \frac{1}{2}\xi_2^2 & \frac{1}{2}\xi_3^2 & \xi_2\xi_3 \\ 0 & 0 & 0 & 1 & 0 & -\xi_3 & 0 & 0 & 0 \\ 0 & 0 & 0 & 0 & 1 & \xi_2 & 0 & 0 & 0 \end{bmatrix},$$

$$\boldsymbol{\varepsilon} = \begin{bmatrix} \epsilon \\ \kappa_2 \\ \kappa_3 \\ \gamma_2 \\ \gamma_3 \\ \kappa_1 \\ \chi_2 \\ \chi_3 \\ \chi_{23} \end{bmatrix} = \begin{bmatrix} \frac{1}{2}\left(\boldsymbol{x}_0' \cdot \boldsymbol{x}_0' - \boldsymbol{X}_0' \cdot \boldsymbol{X}_0'\right) \\ \boldsymbol{x}_0' \cdot \boldsymbol{e}_3' - \boldsymbol{X}_0' \cdot \boldsymbol{E}_3' \\ \boldsymbol{x}_0' \cdot \boldsymbol{e}_2' - \boldsymbol{X}_0' \cdot \boldsymbol{E}_2' \\ \boldsymbol{x}_0' \cdot \boldsymbol{e}_2 - \boldsymbol{X}_0' \cdot \boldsymbol{E}_2 \\ \boldsymbol{x}_0' \cdot \boldsymbol{e}_3 - \boldsymbol{X}_0' \cdot \boldsymbol{E}_3 \\ \boldsymbol{e}_2' \cdot \boldsymbol{e}_3 - \boldsymbol{E}_2' \cdot \boldsymbol{E}_3 \\ \boldsymbol{e}_2' \cdot \boldsymbol{e}_2' - \boldsymbol{E}_2' \cdot \boldsymbol{E}_2' \\ \boldsymbol{e}_3' \cdot \boldsymbol{e}_3' - \boldsymbol{E}_3' \cdot \boldsymbol{E}_3' \\ \boldsymbol{e}_2' \cdot \boldsymbol{e}_3' - \boldsymbol{E}_2' \cdot \boldsymbol{E}_3' \end{bmatrix}. \tag{8}$$

The generalized beam strains belong to a material description and are expressed in a rectangular coordinate system.

Now we introduce a curvilinear coordinate system (x, n, s) and transform the GL strains to this coordinate system, the cross-section shape will be there defined by functions $\bar{\xi}_i(n, s)$. The coordinate s is measured along the tangent to the middle line of the cross-section, in clockwise direction and with origin conveniently chosen. Also, the thickness coordinate $n(-e/2 \leqslant e/2)$ is perpendicular to s and with origin in the middle line contour. To represent the GL strains in this curvilinear coordinate system we make use of a curvilinear transformation tensor $\boldsymbol{P}$, which is formed by the derivatives of the middle line coordinates of the cross-section $\bar{\xi}_i$ as:

$$\boldsymbol{P} = \begin{bmatrix} 1 & 0 & 0 \\ 0 & \frac{d\bar{\xi}_2}{ds} & \frac{d\bar{\xi}_3}{ds} \\ 0 & -\frac{d\bar{\xi}_3}{ds} & \frac{d\bar{\xi}_2}{ds} \end{bmatrix}. \tag{9}$$

The tensor $\boldsymbol{P}$ transforms the rectangular strain measures in intrinsic strain measures; hence the GL strain vector in the curvilinear coordinate system is obtained by transforming the rectangular GL strains as:

$$\widehat{\boldsymbol{E}}_{GL} = [E_{xx}\ 2E_{xs}\ 2E_{xn}]^T = \boldsymbol{P}\ \boldsymbol{E}_{GL} = \boldsymbol{P}\ \boldsymbol{D}\ \boldsymbol{\varepsilon}. \tag{10}$$

The GL strain vector in curvilinear coordinates has the simple closed expression:

$$\widehat{\boldsymbol{E}}_{GL} = \begin{bmatrix} \epsilon + \xi_2\kappa_3 + \xi_3\kappa_2 + \frac{1}{2}\xi_2^2\chi_2 + \frac{1}{2}\xi_3^2\chi_3 + \xi_2\xi_3\chi_{23} \\ \bar{\xi}_2'\gamma_2 + \bar{\xi}_3'\gamma_3 + \left(\xi_2\bar{\xi}_3' - \xi_3\bar{\xi}_2'\right)\kappa_1 \\ -\bar{\xi}_3'\gamma_2 + \bar{\xi}_2'\gamma_3 + \left(\xi_2\bar{\xi}_2' + \xi_3\bar{\xi}_3'\right)\kappa_1 \end{bmatrix}. \tag{11}$$

It must be remembered that $\bar{\xi}_i$ are variables that locates the points lying in the middle-line contour; note that the prime symbol has been used to denote derivation with respect to the coordinate s.

The location of a point anywhere in the cross-section can be expressed as:

$$\xi_2(n, s) = \bar{\xi}_2(s) - n\frac{d\bar{\xi}_3}{ds}, \quad \xi_3(n, s) = \bar{\xi}_3(s) + n\frac{d\bar{\xi}_2}{ds}. \tag{12}$$

The strain state of the composite laminate (see.[39]) will be described by a shell strain vector:

$$\boldsymbol{\epsilon}_s = [\,\varepsilon_{xx} \quad \gamma_{xs} \quad \gamma_{xn} \quad \varkappa_{xx} \quad \varkappa_{xs}\,]^T. \tag{13}$$

Now we introduce Eq. (12) into Eq. (11) to express the GL strains as a function of the mid-surface coordinates $\bar{\xi}_i$ and its derivatives, we find that a matrix $\mathcal{T}$ establish the relationship between the GL curvilinear strains and the generalized strains as:

$$\boldsymbol{\epsilon}_s = \mathcal{T}\ \boldsymbol{\varepsilon}. \tag{14}$$

Substituting Eq. (12) into Eq. (11) and neglecting higher order terms in the thickness (i.e. terms in n^2) we obtain:

$$\mathcal{T}(s) = \begin{bmatrix} 1 & \bar{\xi}_3 & \bar{\xi}_2 & 0 & 0 & 0 & \frac{1}{2}\bar{\xi}_2^2 & \frac{1}{2}\bar{\xi}_3^2 & \bar{\xi}_2\bar{\xi}_3 \\ 0 & 0 & 0 & \bar{\xi}_2' & \bar{\xi}_3' & \bar{\xi}_2\bar{\xi}_3' - \bar{\xi}_3\bar{\xi}_2' & 0 & 0 & 0 \\ 0 & 0 & 0 & -\bar{\xi}_3' & \bar{\xi}_2' & \bar{\xi}_2\bar{\xi}_2' + \bar{\xi}_3\bar{\xi}_3' & 0 & 0 & 0 \\ 0 & \bar{\xi}_2' & -\bar{\xi}_3' & 0 & 0 & 0 & -\bar{\xi}_2\bar{\xi}_3' & \bar{\xi}_3\bar{\xi}_2' & \left(\bar{\xi}_2\bar{\xi}_2' - \bar{\xi}_3\bar{\xi}_3'\right) \\ 0 & 0 & 0 & 0 & 0 & -\left(\bar{\xi}_2'^2 + \bar{\xi}_3'^2\right) & 0 & 0 & 0 \end{bmatrix}. \tag{15}$$

It is noted that the matrix $\mathcal{T}$ plays the role of a double transformation matrix that directly maps the generalized strains ε into the curvilinear GL strain ϵ_s without the need of an intermediate transformation (see Fig. 1).

2.3. Cross-sectional modeling

One of the most important aspects regarding wind turbine blade modeling is the formulation of its cross-sectional stiffness. As it can be seen from Fig. 2, the typical cross-section of a wind turbine blade is highly heterogeneous; this greatly complicates the cross-sectional modeling and a closed form solution for the cross-sectional stiffness matrix is not possible to obtain. As it was said, several methods for the determination of the cross-sectional stiffness can be found in the literature. We propose an approach based on a 1D discretization of the cross-section; this is particularly attractive for optimization studies, since it opens the possibility for using cross-sectional parameters as target functions without re-meshing the beam cross-section.

As it was stated, the present formulation can handle composite materials in a geometrically exact framework without modifying the classical thin-walled beam approach. We have chosen the GL strain as a measure of strain; this implies that we must use a material stress tensor as its work conjugate variable, this is the second Piola-Kirchhoff stress tensor $\boldsymbol{\sigma}$. For an orthotropic lamina, the

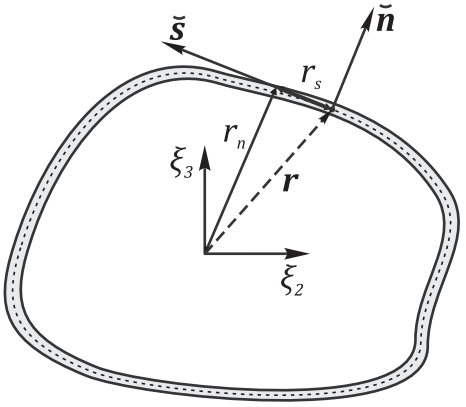

Fig. 1. Curvilinear coordinate system.

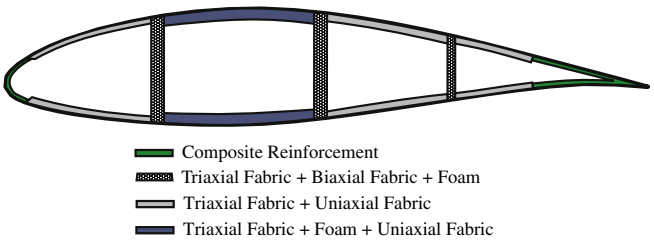

Fig. 2. Wind turbine blade cross-section.

relationship between $\boldsymbol{\sigma}$ and the GL strain tensor, can be expressed in curvilinear coordinates as a matrix of stiffness coefficients Q_{ij} [39,40]:

$$\begin{bmatrix}\sigma_{xx}\\ \sigma_{ss}\\ \sigma_{nn}\\ \sigma_{sn}\\ \sigma_{xn}\\ \sigma_{xs}\end{bmatrix}=\begin{bmatrix}Q_{11} & Q_{12} & Q_{13} & 0 & 0 & Q_{16}\\ Q_{12} & Q_{22} & Q_{23} & 0 & 0 & Q_{26}\\ Q_{13} & Q_{23} & Q_{33} & 0 & 0 & Q_{36}\\ 0 & 0 & 0 & Q_{44} & Q_{45} & 0\\ 0 & 0 & 0 & Q_{45} & Q_{55} & 0\\ Q_{16} & Q_{26} & Q_{36} & 0 & 0 & Q_{66}\end{bmatrix}\begin{bmatrix}\epsilon_{xx}\\ \epsilon_{ss}\\ \epsilon_{nn}\\ \gamma_{sn}\\ \gamma_{xn}\\ \gamma_{xs}\end{bmatrix}, \tag{16}$$

where Q_{ij} are components of the *transformed constitutive (or stiffness) matrix* defined in terms of the elastic properties (elasticity moduli and Poisson coefficients) and fiber orientation of the ply.[39]. In matrix form the above equation takes the form:

$$\boldsymbol{\sigma}=\mathbf{Q}\boldsymbol{\epsilon_s}. \tag{17}$$

Although the last relationships were derived for a single lamina, we can obtain the constitutive relations for a laminate by spanning the integrals in the thickness of the lamina over the different layers of the laminate (each layer being a single lamina). Therefore, using the hypotheses of plane stress in the laminate and plane stress, i.e. $N_{ss}=0$.[39], the constitutive equations for the laminate are:

$$\begin{bmatrix}N_{xx}\\ N_{xs}\\ N_{xn}\\ M_{xx}\\ M_{xs}\end{bmatrix}=\begin{bmatrix}\overline{A}_{11} & \overline{A}_{16} & 0 & \overline{B}_{11} & \overline{B}_{16}\\ \overline{A}_{16} & \overline{A}_{66} & 0 & \overline{B}_{16} & \overline{B}_{66}\\ 0 & 0 & \overline{A}^{H}_{55} & 0 & 0\\ \overline{B}_{11} & \overline{B}_{16} & 0 & \overline{D}_{11} & \overline{D}_{16}\\ \overline{B}_{16} & \overline{B}_{66} & 0 & \overline{D}_{16} & \overline{D}_{66}\end{bmatrix}\begin{bmatrix}\varepsilon_{xx}\\ \gamma_{xs}\\ \gamma_{xn}\\ \chi_{xx}\\ \chi_{xs}\end{bmatrix}, \tag{18}$$

where $\overline{A}_{ij}$ are components of the laminate reduced in-plane stiffness matrix, $\overline{B}_{ij}$ are components of the reduced bending-extension coupling matrix, $\overline{D}_{ij}$ are components of the reduced bending stiffness matrix and $\overline{A}^{H}_{55}$ is the component of the reduced transverse shear stiffness matrix.

We can express the above relation in matrix form as:

$$\boldsymbol{N_s}=\boldsymbol{C}\ \boldsymbol{\epsilon_s}, \tag{19}$$

where $\boldsymbol{C}$ is the composite shell constitutive matrix and $\boldsymbol{\epsilon}_s$ is the curvilinear shell strain vector defined in Eq. (14).

Now, in order to reduce the 2D formulation to a 1D formulation, we express the shell forces as a function of the generalized strains. Replacing Eq. (14) into Eq. (19) we obtain;

$$\boldsymbol{N_s}=\boldsymbol{C}\ \boldsymbol{\mathcal{T}}\ \boldsymbol{\varepsilon}. \tag{20}$$

Now, we transform the shell forces in Eq. (20) back to the "generalized space" by using the double transformation matrix $\boldsymbol{\mathcal{T}}$. Hence, we obtain a sort of the transformed back shell stress as:

$$\boldsymbol{N}^{G}_{s}=\boldsymbol{\mathcal{T}}^{T}\boldsymbol{N}_{s}=\boldsymbol{\mathcal{T}}^{T}\boldsymbol{C}\ \boldsymbol{\mathcal{T}}\ \boldsymbol{\varepsilon}. \tag{21}$$

We see that $\boldsymbol{N}^{G}_{s}$ is a vector of generalized shell stresses defined in the global coordinate system. It is a function of the cross-section mid-contour and thus integration over the contour gives the vector of *generalized beam forces* $\boldsymbol{S}(x)$ (work conjugate with the generalized strains) as:

$$\boldsymbol{S}(x)=\int_{S}\boldsymbol{N}^{G}_{s}ds=\left(\int_{S}\boldsymbol{\mathcal{T}}^{T}\boldsymbol{C}\ \boldsymbol{\mathcal{T}}ds\right)\boldsymbol{\varepsilon}(x)=\mathbb{D}\ \boldsymbol{\varepsilon}(x), \tag{22}$$

$$\mathbb{D}=\int_{S}\boldsymbol{\mathcal{T}}^{T}\boldsymbol{C}\ \boldsymbol{\mathcal{T}}\ ds. \tag{23}$$

The beam constitutive matrix $\mathbb{D}$ is obtained in a closed form or assembled as a sum of one dimensional laminate segments and thus it does not involve a 2D finite element analysis of the cross-section. This method for obtaining the cross-sectional stiffness is very simple and fast. Also, it opens the possibility of addressing optimization problems of large deformation of thin-walled composite beams.

3. Variational equilibrium

The weak form of equilibrium of a three dimensional body $\mathcal{B}$ is given by [41,42]:

$$\delta W(\boldsymbol{\phi},\delta\boldsymbol{\phi})=\int_{\mathcal{B}_0}\boldsymbol{\sigma}\cdot\delta\boldsymbol{\epsilon}\ dV-\int_{\mathcal{B}_0}\boldsymbol{\rho_0 b}\cdot\delta\boldsymbol{\phi}\ dV-\int_{\partial\mathcal{B}_0}(\boldsymbol{p}\cdot\delta\boldsymbol{u}_0+\boldsymbol{m}\cdot\delta\boldsymbol{\theta})d\Omega, \tag{24}$$

where $\boldsymbol{b}$, $\boldsymbol{p}$ and $\boldsymbol{m}$ are: body forces, prescribed external forces and prescribed external moments per unit length respectively. $\boldsymbol{\epsilon}$ is the GL strain tensor, work conjugate to the second Piola-Kirchhoff stress tensor $\boldsymbol{\sigma}$. Where $\boldsymbol{\sigma}$ could be defined in either a rectangular or a curvilinear coordinate system (such a distinction is, at least here, unnecessary).

3.1. The virtual strains

The admissible variation of the director field is required to obtain the variation of the generalized strains. From Eq. (1), we can write:

$$\delta\boldsymbol{e}_i=\delta(\boldsymbol{\Lambda}(x)\boldsymbol{E}_i)=\delta\boldsymbol{\Lambda}(x)\boldsymbol{E}_i. \tag{25}$$

The admissible variation of the rotation tensor (Lie variation) is obtained by superposing an infinitesimal virtual rotation onto the existing finite rotation, see e.g. [10,43]. This virtual rotation can belong to a material vector space or a spatial vector space, they will be called $\delta\boldsymbol{\Theta}$ and $\delta\boldsymbol{w}$ respectively. It is interesting to note that both virtual rotations are elements of the tangent space at $\boldsymbol{\Lambda}$, i.e. $T_{\boldsymbol{\Lambda}}SO(3)$, $\delta\boldsymbol{\Theta}\in T^{mat}_{\boldsymbol{\Lambda}}$ and $\delta\boldsymbol{w}\in T^{spat}_{\boldsymbol{\Lambda}}$. Both virtual rotation vectors are often called *spins*.

Considering the latter we can construct a perturbed rotation tensor by using either the spatial or the material form of compound rotation as:

$$\boldsymbol{\Lambda}_{\epsilon}=exp(\epsilon\delta\tilde{\boldsymbol{w}})\boldsymbol{\Lambda}=\boldsymbol{\Lambda}exp(\epsilon\delta\widetilde{\boldsymbol{\Theta}}), \tag{26}$$

where $\tilde{}$ indicates the skew symmetric matrix of a vector $\boldsymbol{b}$ such that $\tilde{\boldsymbol{b}}\boldsymbol{a}=\boldsymbol{b}\times\boldsymbol{a}$. Now, by making use of the cartesian rotation vector, we can propose:

$$\boldsymbol{\Lambda}_{\epsilon}=exp(\tilde{\boldsymbol{\theta}}+\epsilon\delta\tilde{\boldsymbol{\theta}}), \tag{27}$$

and try to find an incremental rotation tensor $\delta\tilde{\boldsymbol{\theta}}$ such that it belongs to the same tangent space as the rotation tensor $\tilde{\boldsymbol{\theta}}$, i.e. $T_{I}SO(3)$. Recalling Eq. (26) for the material virtual rotation tensor and recalling that $\boldsymbol{\Lambda}=exp(\tilde{\boldsymbol{\theta}})$ we have:

$$exp(\tilde{\boldsymbol{\theta}}+\epsilon\delta\tilde{\boldsymbol{\theta}})=exp(\tilde{\boldsymbol{\theta}})exp(\epsilon\delta\widetilde{\boldsymbol{\Theta}}). \tag{28}$$

By taking derivatives with respect to the parameter ϵ at $\epsilon=0$ we can obtain (see e.g. [8,44]):

$$\delta\boldsymbol{\Theta}=\boldsymbol{T}\delta\boldsymbol{\theta},\quad \delta\boldsymbol{w}=\boldsymbol{T}^{T}\delta\boldsymbol{\theta}, \tag{29}$$

where $\boldsymbol{T}=\boldsymbol{T}(\boldsymbol{\theta})$ is a linear mapping between the tangent spaces $T^{spat}_{\boldsymbol{I}}SO(3)\rightarrow T^{spat}_{\boldsymbol{\Lambda}}SO(3)$ [2]. Note that, unlike $\boldsymbol{\Lambda}$, $\boldsymbol{T}$ changes the base point $\boldsymbol{I}$ into $\boldsymbol{\Lambda}$.

Now, recalling Eq. (26) we obtain the kinematically admissible variation of the rotation tensor as:

$$\delta\boldsymbol{\Lambda}=\frac{d}{d\epsilon}[\boldsymbol{\Lambda}exp(\epsilon\delta\widetilde{\boldsymbol{\Theta}})]|_{\epsilon=0}=\boldsymbol{\Lambda}\delta\widetilde{\boldsymbol{\Theta}}=\delta\tilde{\boldsymbol{w}}\boldsymbol{\Lambda}. \tag{30}$$

From the last equation it is straightforward to verify that $\delta\widetilde{\boldsymbol{\Theta}}=\boldsymbol{\Lambda}^{T}\delta\tilde{\boldsymbol{w}}\boldsymbol{\Lambda}$. Therefore, we can recall Eq. (25) to write:

$$\delta \boldsymbol{e}_i = \boldsymbol{\Lambda}(\delta\boldsymbol{\Theta} \times \boldsymbol{E}_i) = \delta\boldsymbol{w} \times \boldsymbol{e}_i. \tag{31}$$

Now, recalling Eq. (29), we can write the last equation as a function of the total rotation vector like:

$$\delta \boldsymbol{e}_i = (\boldsymbol{T}^T \delta\boldsymbol{\theta}) \times \boldsymbol{e}_i. \tag{32}$$

Noting that $\boldsymbol{e}' = \widetilde{\boldsymbol{T}^T\boldsymbol{\theta}'}\boldsymbol{e}$ we can find the variation of the director's derivative as:

$$\delta \boldsymbol{e}_i' = (\delta\boldsymbol{T}^T\boldsymbol{\theta}' + \boldsymbol{T}^T\delta\boldsymbol{\theta}') \times \boldsymbol{e}_i + (\boldsymbol{T}^T\boldsymbol{\theta}') \times [(\boldsymbol{T}^T\delta\boldsymbol{\theta}) \times \boldsymbol{e}_i]. \tag{33}$$

The set of kinematically admissible variations can now be defined as:

$$\delta\mathcal{V} := \{\delta\boldsymbol{\phi} = [\delta\boldsymbol{u}_0, \delta\boldsymbol{\theta}]^T : [0,\ell] \to R^3 | \delta\boldsymbol{\phi} = 0 \text{ on } \mathcal{S}\}, \tag{34}$$

where $\mathcal{S}$ describes de boundaries with prescribed displacements and rotations.

The variations of the directors and its derivatives are now used to obtain the virtual generalized strains. Considering that $\delta\,\boldsymbol{E}_i = 0$ and that $\delta\boldsymbol{X}_0' = 0$, and performing the variation to Eq. (8) we obtain:

$$\delta\boldsymbol{\varepsilon} = \begin{bmatrix} \boldsymbol{x}_0' \cdot \delta\boldsymbol{u}_0' \\ \boldsymbol{e}_3' \cdot \delta\boldsymbol{u}_0' + \boldsymbol{x}_0' \cdot \delta\boldsymbol{e}_3' \\ \boldsymbol{e}_2' \cdot \delta\boldsymbol{u}_0' + \boldsymbol{x}_0' \cdot \delta\boldsymbol{e}_2' \\ \boldsymbol{e}_2 \cdot \delta\boldsymbol{u}_0' + \boldsymbol{x}_0' \cdot \delta\boldsymbol{e}_2 \\ \boldsymbol{e}_3 \cdot \delta\boldsymbol{u}_0' + \boldsymbol{x}_0' \cdot \delta\boldsymbol{e}_3 \\ \delta\boldsymbol{e}_2' \cdot \boldsymbol{e}_3 + \boldsymbol{e}_2' \cdot \delta\boldsymbol{e}_3 \\ 2(\delta\boldsymbol{e}_2' \cdot \boldsymbol{e}_2') \\ 2(\delta\boldsymbol{e}_3' \cdot \boldsymbol{e}_3') \\ \delta\boldsymbol{e}_2' \cdot \boldsymbol{e}_3' + \boldsymbol{e}_2' \cdot \delta\boldsymbol{e}_3' \end{bmatrix}. \tag{35}$$

To maintain the compactness of the formulation, it will be useful to write the last expression as a function of a new set of intermediate variables $\delta\boldsymbol{\varphi}$ as:

$$\delta\boldsymbol{\varepsilon} = \mathbb{H}\delta\boldsymbol{\varphi}, \tag{36}$$

where

$$\mathbb{H} = \begin{bmatrix} \boldsymbol{x}_0'^T & \boldsymbol{0} & \boldsymbol{0} & \boldsymbol{0} & \boldsymbol{0} & \boldsymbol{0} \\ \boldsymbol{e}_3'^T & \boldsymbol{0} & \boldsymbol{0} & \boldsymbol{0} & \boldsymbol{0} & \boldsymbol{x}_0'^T \\ \boldsymbol{e}_2'^T & \boldsymbol{0} & \boldsymbol{0} & \boldsymbol{0} & \boldsymbol{x}_0'^T & \boldsymbol{0} \\ \boldsymbol{e}_2^T & \boldsymbol{0} & \boldsymbol{x}_0'^T & \boldsymbol{0} & \boldsymbol{0} & \boldsymbol{0} \\ \boldsymbol{e}_3^T & \boldsymbol{0} & \boldsymbol{0} & \boldsymbol{x}_0'^T & \boldsymbol{0} & \boldsymbol{0} \\ \boldsymbol{0} & \boldsymbol{0} & \boldsymbol{0} & \boldsymbol{e}_2'^T & \boldsymbol{e}_3^T & \boldsymbol{0} \\ \boldsymbol{0} & \boldsymbol{0} & \boldsymbol{0} & \boldsymbol{0} & \boldsymbol{e}_2'^T & \boldsymbol{0} \\ \boldsymbol{0} & \boldsymbol{0} & \boldsymbol{0} & \boldsymbol{0} & \boldsymbol{0} & \boldsymbol{e}_3'^T \\ \boldsymbol{0} & \boldsymbol{0} & \boldsymbol{0} & \boldsymbol{0} & \boldsymbol{e}_3'^T & \boldsymbol{e}_2'^T \end{bmatrix}, \quad \delta\boldsymbol{\varphi} = \begin{bmatrix} \delta\boldsymbol{u}_0' \\ \delta\boldsymbol{\theta} \\ \delta\boldsymbol{e}_2 \\ \delta\boldsymbol{e}_3 \\ \delta\boldsymbol{e}_2' \\ \delta\boldsymbol{e}_3' \end{bmatrix}. \tag{37}$$

3.2. Virtual work of internal and inertia forces

Recalling Eq. (24), the first term can be written in its shell form as:

$$\delta W_i(\boldsymbol{\phi}, \delta\boldsymbol{\phi}) = \int_\ell \int_S \delta\boldsymbol{\epsilon}_s^T\, \boldsymbol{N}_s\, ds\, dx. \tag{38}$$

The reduction to a one dimensional formulation is now aided by the deduction of 1D beam forces presented in Eq. (22). Transforming the virtual curvilinear shell strains into virtual generalized strains we can rewrite the last expression as:

$$\delta W_i(\boldsymbol{\phi}, \delta\boldsymbol{\phi}) = \int_\ell \delta\boldsymbol{\varepsilon}^T \left(\int_S \boldsymbol{\mathcal{T}}^T\, \boldsymbol{N}_s ds \right) dx. \tag{39}$$

In which the term in parentheses is the generalized beam forces vector $\boldsymbol{S}(x)$ (see Eq. (22)). Lastly, we write the one dimensional version of the virtual work principle in terms of the generalized strains and the generalized beam forces:

$$\delta W_i(\boldsymbol{\phi}, \delta\boldsymbol{\phi}) = \int_\ell \delta\boldsymbol{\varepsilon}^T \boldsymbol{S}\, dx. \tag{40}$$

The virtual work of external forces can be written as:

$$\delta W_e(\boldsymbol{\phi}, \delta\boldsymbol{\phi}) = \int_l (\bar{\boldsymbol{n}} \cdot \delta\boldsymbol{u}_0 + \bar{\boldsymbol{m}} \cdot \delta\boldsymbol{\theta}) dx, \tag{41}$$

where $\bar{\boldsymbol{n}}$ is the external forces vector and $\bar{\boldsymbol{m}}$ the external moments vector. These vectors are defined according to:

$$\begin{aligned} \bar{\boldsymbol{n}} &= \int_S \int_e \boldsymbol{b}\, dn\, ds + \int_S \boldsymbol{t}\, ds + \boldsymbol{F}_i, \\ \bar{\boldsymbol{m}} &= \int_S \int_e \boldsymbol{X} \times \boldsymbol{b}\, dn\, ds + \int_S \boldsymbol{X} \times \boldsymbol{t}\, ds + \boldsymbol{M}_i, \end{aligned} \tag{42}$$

where $\boldsymbol{b}$ is the distributed body force vector and $\boldsymbol{t}$ is external stress vector and $\boldsymbol{F}_i$ and $\boldsymbol{M}_i$ are point loads and moments.

Next we derive the virtual work of the inertia forces. Since they play a key role in the dynamics of the multibody system, its treatment should be fully consistent with the geometrical hypotheses of the preceding theory.

Of course both a material and a spatial approach can be used to obtain the virtual work of the inertia forces; it is often preferred to use the material version in order to avoid the Lie derivative in the linearization process, we stick to that approach in what follows.

The inertial virtual work of the beam is expressed as:

$$\delta W_a(\boldsymbol{\phi}, \delta\boldsymbol{\phi}) = \int_{\mathcal{B}_0} \rho_0 \delta\boldsymbol{x}^T \ddot{\boldsymbol{x}}\, dx. \tag{43}$$

Using a material description the virtual configuration and acceleration give:

$$\begin{aligned} \delta\boldsymbol{x} &= \delta\boldsymbol{x}_0 + \delta\boldsymbol{\Lambda}\boldsymbol{\xi} = \delta\boldsymbol{x}_0 + \boldsymbol{\Lambda}\delta\widetilde{\boldsymbol{\Theta}}\boldsymbol{\xi} \\ \ddot{\boldsymbol{x}} &= \ddot{\boldsymbol{x}}_{\boldsymbol{0}} + \ddot{\boldsymbol{\Lambda}}\boldsymbol{\xi} = \ddot{\boldsymbol{x}}_{\boldsymbol{0}} + (\boldsymbol{\Lambda}\widetilde{\boldsymbol{\Omega}}\widetilde{\boldsymbol{\Omega}} + \boldsymbol{\Lambda}\dot{\widetilde{\boldsymbol{\Omega}}})\boldsymbol{\xi}. \end{aligned} \tag{44}$$

We can operate over the last expression to obtain:

$$\delta W_a(\boldsymbol{\phi}, \delta\boldsymbol{\phi}) = \int_{\mathcal{B}_0} \rho_0 (\delta\boldsymbol{x}_0 + \boldsymbol{\Lambda}\delta\widetilde{\boldsymbol{\Theta}}\boldsymbol{\xi})^T [\ddot{\boldsymbol{x}}_{\boldsymbol{0}} + (\boldsymbol{\Lambda}\widetilde{\boldsymbol{\Omega}}\widetilde{\boldsymbol{\Omega}} + \boldsymbol{\Lambda}\dot{\widetilde{\boldsymbol{\Omega}}})\boldsymbol{\xi}] dx. \tag{45}$$

Integrating over the cross-section we obtain:

$$\delta W_a(\boldsymbol{\phi}, \delta\boldsymbol{\phi}) = \int_l m(\delta\boldsymbol{x}_0^T \ddot{\boldsymbol{x}}_{\boldsymbol{0}}) + \delta\boldsymbol{\Theta}^T(\boldsymbol{J}\dot{\boldsymbol{\Omega}} + \widetilde{\boldsymbol{\Omega}}\boldsymbol{J}\,\boldsymbol{\Omega}) dx, \tag{46}$$

where we have assumed that pole (reference point) of the cross-section is coincident with the center of mass, then $\int_A \xi dA = 0$. Therefore, the cross-sectional mass and constant inertia tensors are given by:

$$m = \int_A \rho_0\, dA, \quad \boldsymbol{J} = \int_A \rho_0 \tilde{\boldsymbol{\xi}}^T \tilde{\boldsymbol{\xi}} dA, \tag{47}$$

where ρ is the material density. It is interesting to note that the constant inertia tensor is characteristic of material descriptions.

4. Linearized equilibrium equations

The linearization of the equilibrium equations is necessary to solve the nonlinear system of equation by means of the Newton method. The linearization of the variational equilibrium equations is obtained through the directional derivative and, assuming conservative loading, its application gives four tangent terms; the material and the geometric stiffness matrices, the mass tangent matrix and the load tangent matrix.

Applying the directional derivative in the direction $\Delta\boldsymbol{\phi}$ to the internal virtual work and recalling Eqs. (40) and (35), we obtain the tangent stiffness as:

$$\mathcal{D}\delta W_i(\boldsymbol{\phi},\delta\boldsymbol{\phi})\cdot\Delta\boldsymbol{\phi}=\int_\ell(\delta\boldsymbol{\varepsilon}^T\mathbb{D}\Delta\boldsymbol{\varepsilon}+\Delta\delta\boldsymbol{\varepsilon}^T\boldsymbol{S})dx, \tag{48}$$

where ℓ is the length of the undeformed beam and $\mathcal{D}$ indicates directional derivative.

Using Eq. (36) the first term of the right hand side of the above equation gives de material stiffness terms as:

$$\mathcal{D}_1\delta W_i(\boldsymbol{\phi},\delta\boldsymbol{\phi})\cdot\Delta\boldsymbol{\phi}=\int_\ell\delta\boldsymbol{\varphi}^T\mathbb{H}^T\mathbb{D}\mathbb{H}\Delta\boldsymbol{\varphi}\,dx. \tag{49}$$

On the other hand, from the second term, the general expression of the geometric stiffness operator gives:

$$\mathcal{D}_2\delta W_i(\boldsymbol{\phi},\delta\boldsymbol{\phi})\cdot\Delta\boldsymbol{\phi}=\int_\ell\Delta\delta\boldsymbol{\varepsilon}^T\boldsymbol{S}\,dx. \tag{50}$$

The linearization of the virtual generalized strains is:

$$\Delta\delta\boldsymbol{\varepsilon}=\begin{bmatrix}\delta\boldsymbol{u}'\cdot\Delta\boldsymbol{u}_0'\\ \delta\boldsymbol{u}_0'\cdot\Delta\boldsymbol{e}_3'+\delta\boldsymbol{e}_3'\cdot\Delta\boldsymbol{u}_0'+\boldsymbol{x}_0'\cdot\Delta\delta\boldsymbol{e}_3'\\ \delta\boldsymbol{u}_0'\cdot\Delta\boldsymbol{e}_2'+\delta\boldsymbol{e}_2'\cdot\Delta\boldsymbol{u}_0'+\boldsymbol{x}_0'\cdot\Delta\delta\boldsymbol{e}_2'\\ \delta\boldsymbol{u}_0'\cdot\Delta\boldsymbol{e}_2+\delta\boldsymbol{e}_2\cdot\Delta\boldsymbol{u}_0'+\boldsymbol{x}_0'\cdot\Delta\delta\boldsymbol{e}_2\\ \delta\boldsymbol{u}_0'\cdot\Delta\boldsymbol{e}_3+\delta\boldsymbol{e}_3\cdot\Delta\boldsymbol{u}_0'+\boldsymbol{x}_0'\cdot\Delta\delta\boldsymbol{e}_3\\ \delta\boldsymbol{e}_2'\cdot\Delta\boldsymbol{e}_3+\delta\boldsymbol{e}_3\cdot\Delta\boldsymbol{e}_2'+\boldsymbol{e}_3\cdot\Delta\delta\boldsymbol{e}_2'+\boldsymbol{e}_2'\cdot\Delta\delta\boldsymbol{e}_3\\ 2\left(\boldsymbol{e}_2'\cdot\Delta\delta\boldsymbol{e}_2'+\delta\boldsymbol{e}_2'\cdot\Delta\boldsymbol{e}_2'\right)\\ 2\left(\boldsymbol{e}_3'\cdot\Delta\delta\boldsymbol{e}_3'+\delta\boldsymbol{e}_3'\cdot\Delta\boldsymbol{e}_3'\right)\\ \delta\boldsymbol{e}_2'\cdot\Delta\boldsymbol{e}_3'+\delta\boldsymbol{e}_3'\cdot\Delta\boldsymbol{e}_2'+\boldsymbol{e}_3'\cdot\Delta\delta\boldsymbol{e}_2'+\boldsymbol{e}_2'\cdot\Delta\delta\boldsymbol{e}_3'\end{bmatrix}. \tag{51}$$

To complete de development of the geometric stiffness matrix, we need to find the linearization of the virtual generalized strains, i.e. $\Delta\delta\boldsymbol{\varepsilon}^T$, for what we first need to obtain the linearized virtual directors. Using Eq. (32), the linearization of the virtual directors can be obtained as:

$$\Delta\delta\boldsymbol{e}_i=(\Delta\boldsymbol{T}^T\delta\boldsymbol{\theta})\times\boldsymbol{e}_i+(\boldsymbol{T}^T\delta\boldsymbol{\theta})\times[(\boldsymbol{T}^T\Delta\boldsymbol{\theta})\times\boldsymbol{e}_i]. \tag{52}$$

Now we need to linearize the virtual work of the inertia forces. Using Eq. (29) we can obtain the angular velocity and angular acceleration spin vectors as:

$$\boldsymbol{\Omega}=\boldsymbol{T}\,\dot{\boldsymbol{\theta}},\quad \boldsymbol{\Omega}=\dot{\boldsymbol{T}}\,\dot{\boldsymbol{\theta}}+\boldsymbol{T}\,\ddot{\boldsymbol{\theta}}. \tag{53}$$

Replacing the above expression into the expression (46) we obtain:

$$\delta W_a(\boldsymbol{\phi},\delta\boldsymbol{\phi})=\int_l\boldsymbol{m}(\delta\boldsymbol{x}_0^T\ddot{\boldsymbol{x}}_0)+\delta\boldsymbol{\theta}^T(\boldsymbol{T}^T\boldsymbol{J}\,\dot{\boldsymbol{T}}\,\dot{\boldsymbol{\theta}}+\boldsymbol{T}^T\boldsymbol{J}\,\boldsymbol{T}\,\ddot{\boldsymbol{\theta}}+\boldsymbol{T}^T\,(\widetilde{\boldsymbol{T}\dot{\boldsymbol{\theta}}})\boldsymbol{J}\,\boldsymbol{T}\,\dot{\boldsymbol{\theta}})dx. \tag{54}$$

The last expression is already in linear form with respect to the acceleration field $\ddot{\boldsymbol{\phi}}$, so its linearization involves only the linearization with respect to a change in configuration and velocities:

$$\mathcal{D}\delta W_a(\boldsymbol{\phi},\delta\boldsymbol{\phi})\cdot[\Delta(\boldsymbol{\phi},\dot{\boldsymbol{\phi}},\ddot{\boldsymbol{\phi}})]=\mathcal{D}\delta W_a\cdot[\Delta\boldsymbol{\phi}]+\mathcal{D}\delta W_a\cdot[\Delta\dot{\boldsymbol{\phi}}]+\int_l\delta\boldsymbol{\phi}^T\mathbb{M}\Delta\ddot{\boldsymbol{\phi}}. \tag{55}$$

In the above equation, the mass matrix is:

$$\mathbb{M}=\begin{bmatrix}\boldsymbol{m} & \boldsymbol{0}\\ \boldsymbol{0} & \boldsymbol{T}^T\boldsymbol{J}\,\boldsymbol{T}\end{bmatrix}, \tag{56}$$

where $\boldsymbol{m}=m\boldsymbol{I}$, being $\boldsymbol{I}$ is the 3×3 identity matrix.

The linearization of the virtual work of the inertia forces in the directions $\Delta\boldsymbol{\phi}$ and $\Delta\dot{\boldsymbol{\phi}}$ give raise to centrifugal and gyroscopic inertia matrices. Numerical tests to be presented in a future work confirm that centrifugal and gyroscopic inertia effects are negligible, this preliminary conclusion is in line with the observations made in [45]. Because it is costly to evaluate the complex matrices that evolve from the treatment of these effects, they will be disregarded hereon. Thus, the linearized version of the virtual work of the inertia forces reduces to:

$$\mathcal{D}\delta W_a(\boldsymbol{\phi},\delta\boldsymbol{\phi})\cdot[\Delta(\boldsymbol{\phi},\dot{\boldsymbol{\phi}},\ddot{\boldsymbol{\phi}})]=\int_l\delta\boldsymbol{\phi}^T\mathbb{M}\Delta\ddot{\boldsymbol{\phi}}. \tag{57}$$

Now, the linearization of the virtual work of the external forces gives raise to the tangent load stiffness; only the case of conservative loading makes this stiffness zero. Clearly, for wind turbine applications the case of conservative loading is too restrictive since the aerodynamic loading is of course nonconservative.

Adopting a spatial description and integrating distributed forces and moments we can express the virtual work of external forces (41) as:

$$\delta W_e(\boldsymbol{\phi},\delta\boldsymbol{\phi})=\int_L\delta\boldsymbol{x}_c^T(\overline{\boldsymbol{F}}+\overrightarrow{\boldsymbol{F}})dV+\int_L\delta\boldsymbol{\theta}^T(\overline{\boldsymbol{M}}+\overrightarrow{\boldsymbol{M}}+\overline{\overline{\boldsymbol{M}}})\boldsymbol{dV}, \tag{58}$$

where $\overline{\boldsymbol{F}}$ and $\overrightarrow{\boldsymbol{F}}$ are fixed and follower forces respectively and $\overline{\boldsymbol{M}}$, $\overrightarrow{\boldsymbol{M}}$ and $\overline{\overline{\boldsymbol{M}}}$ represent moment related quantities associated to fixed moments, follower moments and imposed moments respectively [46]. Assuming that moments can be generated either by eccentric forces or point torques, the last expression gives:

$$\delta W_e=\int_L\delta\boldsymbol{x}_c^T(\overline{\boldsymbol{P}}+\boldsymbol{\Lambda}\overrightarrow{\boldsymbol{P}})dV+\int_L\delta\boldsymbol{\theta}^T(\boldsymbol{T}^T\tilde{\boldsymbol{\xi}}\boldsymbol{\Lambda}^T\overline{\boldsymbol{P}}+\boldsymbol{T}^T\tilde{\boldsymbol{\xi}}\overrightarrow{\boldsymbol{P}}+T\bar{\boldsymbol{m}})dV, \tag{59}$$

where $\overline{\boldsymbol{P}}$ and $\overrightarrow{\boldsymbol{P}}$ are the initial components of the fixed and follower forces and $\bar{\boldsymbol{m}}$ is the applied point torque.

Assuming that the external forces are not dissipative, the linearization of its virtual work can be obtained as:

$$\mathcal{D}\delta W_e(\boldsymbol{\phi},\delta\boldsymbol{\phi})\cdot[\Delta(\boldsymbol{\phi},\dot{\boldsymbol{\phi}},\ddot{\boldsymbol{\phi}})]=\mathcal{D}\delta W_e(\boldsymbol{\phi},\delta\boldsymbol{\phi})\cdot[\Delta\boldsymbol{\phi}], \tag{60}$$

it gives:

$$\mathcal{D}\delta W_e(\boldsymbol{\phi},\delta\boldsymbol{\phi})\cdot[\Delta\boldsymbol{\phi}]=\int_L\delta\boldsymbol{x}_c^T\Delta\boldsymbol{\Lambda}\overrightarrow{\boldsymbol{P}}dV+\int_L\delta\boldsymbol{\theta}^T(\Delta\boldsymbol{T}^T\tilde{\boldsymbol{\xi}}\boldsymbol{\Lambda}^T\overline{\boldsymbol{P}}+\boldsymbol{T}^T\tilde{\boldsymbol{\xi}}\Delta\boldsymbol{\Lambda}^T\overline{\boldsymbol{P}}+\Delta\boldsymbol{T}^T\tilde{\boldsymbol{\xi}}\overrightarrow{\boldsymbol{P}}+\Delta\boldsymbol{T}\bar{\boldsymbol{m}})dV. \tag{61}$$

It is possible to write the last expression as:

$$\mathcal{D}\delta W_e(\boldsymbol{\phi},\delta\boldsymbol{\phi})\cdot[\Delta\boldsymbol{\phi}]=\int_L\delta\boldsymbol{\phi}^T\mathbb{L}\Delta\boldsymbol{\phi}dx,\qquad \mathbb{L}=\begin{bmatrix}0 & \boldsymbol{\Xi}_\Lambda(\overrightarrow{\boldsymbol{P}})\\ 0 & \boldsymbol{\Xi}_{\boldsymbol{T}^T}(\tilde{\boldsymbol{\xi}}\boldsymbol{\Lambda}^T\overline{\boldsymbol{P}})+\boldsymbol{T}^T\tilde{\boldsymbol{\xi}}\boldsymbol{\Xi}_{\boldsymbol{\Lambda}^T}(\overline{\boldsymbol{P}})+\boldsymbol{\Xi}_{\boldsymbol{T}^T}(\tilde{\boldsymbol{\xi}}\overrightarrow{\boldsymbol{P}})+\boldsymbol{\Xi}_T(\bar{\boldsymbol{m}})\end{bmatrix}, \tag{62}$$

being $\boldsymbol{\Xi}_A$ and operator such that for any matrix $\boldsymbol{A}$ and any vector $\boldsymbol{b}$:

$$\boldsymbol{\Xi}_{\boldsymbol{A}}(\boldsymbol{b})\cdot[\Delta\boldsymbol{\phi}]=\mathcal{D}[\boldsymbol{A}(\boldsymbol{b})]\cdot[\Delta\boldsymbol{\phi}]. \tag{63}$$

As it can be seen from the expression of the operator $\mathbb{L}$, there exist linearization terms for all external loading except for the case of noneccentric fixed forces; except for this case, all the loading is nonconservative.

5. Finite element formulation

As it was mentioned, the finite element implementation is based on an Updated Lagrangian procedure; some aspects are similar to that of the Total Lagrangian implementation in [13] and will be omitted. The main motivation for the proposition of an Updated Lagrangian formulation is due to the fact that the updating procedure can effectively avoid the singularities that arise when the rotation vector modulus is near 2π. In the present formulation, after each time step the rotation vector is set to zero and the total rotation is stored as the reference rotation of the next time step. Contrary to the mentioned procedure for the rotation vector, the director field is updated iteratively, so it has always a total (spatial) meaning.

In the present implementation two triads per element (one for each node) form the basis for the intermediate kinematic variables; see Fig. 3. Thus, the obtention of the derivatives of the director field can be obtained by interpolation.

The director field is updated iteratively at the nodes using an incremental scheme as:

$$\hat{\boldsymbol{e}}_i^{t+1} = \boldsymbol{\Lambda}_{\Delta}(\boldsymbol{\theta})\hat{\boldsymbol{e}}_i^{t}, \tag{64}$$

where $\hat{\boldsymbol{e}}_i^{t+1}$ is the vector i of the director triad at time $t+1$, $\hat{\boldsymbol{e}}_i^{t}$ is the vector i of the director triad at time t and $\boldsymbol{\Lambda}_{\Delta}(\boldsymbol{\theta})$ is the incremental rotation tensor. The nodal triads give us the possibility to approximate the derivative of the director field as:

$$\boldsymbol{e}_i'^{n+1} \cong \sum_{j=1}^{nn} N_j' \hat{\boldsymbol{e}}_i^{j\ n+1}. \tag{65}$$

5.1. Interpolation and directors update

The finite element implementation is based on linear interpolation and one point reduced integration; thus avoiding shear locking. A relevant procedure of the finite element implementation is the use of interpolation to obtain the derivatives of the director field, this greatly simplifies the expression of the tangent stiffness matrix. It must be noted that although the interpolation operation causes the orthonormality property of the interpolated triad to be lost, this is not a drawback since the generalized deformations are evaluated in a Total sense. This is, deformations are calculated from nodal triads and after the iteration process the interpolated triads are discarded.

We interpolate the position vectors in the undeformed and deformed configuration as:

$$\boldsymbol{X} = \sum_{j=1}^{nn} N_j \widehat{\boldsymbol{X}}_j, \quad \boldsymbol{x} = \sum_{j=1}^{nn} N_j(\widehat{\boldsymbol{X}}_j + \hat{\boldsymbol{u}}_j), \tag{66}$$

where $\wedge$ indicates a nodal value, j is the node index and nn is the number of nodes per element. Also, we define:

$$\boldsymbol{N}_j = \begin{bmatrix} N_j & 0 & 0 \\ 0 & N_j & 0 \\ 0 & 0 & N_j \end{bmatrix}, \quad \mathbb{N}_j = \begin{bmatrix} \boldsymbol{N}_j & \boldsymbol{0} \\ \boldsymbol{0} & \boldsymbol{N}_j \end{bmatrix}. \tag{67}$$

The same interpolation is also applied to the configuration and its variation, so:

$$\begin{aligned} \boldsymbol{\phi} &= \sum_{j=1}^{nn} N_j \hat{\boldsymbol{\phi}}_j, \quad \boldsymbol{\phi}' = \sum_{j=1}^{nn} N_j' \hat{\boldsymbol{\phi}}_j, \quad \delta\boldsymbol{\phi} = \sum_{j=1}^{nn} N_j \delta\hat{\boldsymbol{\phi}}_j, \quad \delta\boldsymbol{\phi}' \\ &= \sum_{j=1}^{nn} N_j' \delta\hat{\boldsymbol{\phi}}_j. \end{aligned} \tag{68}$$

A simple way to obtain the derivatives of the director field is to use interpolation. So, being N_j linear Lagrangian shape function coefficients, it will be assumed that:

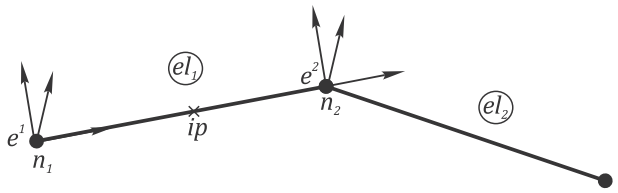

Fig. 3. Updated Lagrangian finite element.

$$\boldsymbol{e}_i' \cong \sum_{j=1}^{nn} N_j' \hat{\boldsymbol{e}}_i^{j}, \tag{69}$$

where $\hat{\boldsymbol{e}}_i^{j}$ stands for the director i at the node j and nn is the number of nodes per element, which in the present case is 2.

It is very important to observe that the use of interpolation of triads to obtain the derivatives of the director field actually causes a minor loss of accuracy in the evaluation of the deformation state of the element if compared to that given by the use of derivation of the right hand side of Eq. (1), as done in the Eulerian formulation developed in [11]. This drawback disappears as the mesh is refined, then the deformation state converge to that of the Eulerian formulation; for the present application we assume that the shape change of the cross-section impose a restriction on the element length that precludes the emergence of the mentioned accuracy problem

5.2. Discrete virtual directors

Assuming holonomic constraints we may interchange variations and derivatives, i.e. $\delta(\boldsymbol{e}') = (\delta\boldsymbol{e})'$. Using this property, we can use Eq. (69) to obtain the variation of the directors and its derivatives as:

$$\delta\boldsymbol{e}_i \cong \sum_{j=1}^{nn} N_j \delta\hat{\boldsymbol{e}}_i^{j}, \quad \delta\boldsymbol{e}_i' \cong \sum_{j=1}^{nn} N_j' \delta\hat{\boldsymbol{e}}_i^{j}. \tag{70}$$

The obtention of the linearization of the directors and its derivatives is more involved and requires the linearization of the tangential transformation. Observing the linearization of the variation of the directors appears in the virtual strains (and also in its linearization) always pre multiplied by some constant vector $\boldsymbol{a}$, for simplicity in the arranging of terms, it is preferable to obtain the expression for this product and not only for the second variation. Thus, recalling Eq. (52), we find that:

$$\boldsymbol{a}\cdot\Delta\delta\boldsymbol{e}_i = \boldsymbol{a}\cdot\left\{\left(\Delta\boldsymbol{T}_{\Delta}^{T}\delta\boldsymbol{\theta}\right)\times\boldsymbol{e}_i + \left(\boldsymbol{T}_{\Delta}^{T}\delta\boldsymbol{\theta}\right)\times\left[\left(\boldsymbol{T}_{\Delta}^{T}\Delta\boldsymbol{\theta}\right)\times\boldsymbol{e}_i\right]\right\}. \tag{71}$$

Switching to matrix notation, using spinors in place of cross-products and reordering some terms we can re-write the above equation as:

$$\boldsymbol{a}\cdot\Delta\delta\boldsymbol{e}_i = \delta\boldsymbol{\theta}^{T}\Delta\boldsymbol{T}_{\Delta}(\tilde{\boldsymbol{e}}_i\boldsymbol{a}) + \delta\boldsymbol{w}^{T}(\tilde{\boldsymbol{a}}\tilde{\boldsymbol{e}}_i)\Delta\boldsymbol{w}, \tag{72}$$

where $\tilde{\hat{\boldsymbol{e}}}_i^{j}$ is the spinor of the director i at node j and:

$$\Delta\boldsymbol{T}_{\Delta}(\tilde{\boldsymbol{e}}_i\boldsymbol{a}) = D[\boldsymbol{T}_{\Delta}(\tilde{\boldsymbol{e}}_i\boldsymbol{a})]\cdot\Delta\boldsymbol{\theta}. \tag{73}$$

The linearization of the term $\boldsymbol{T}_{\Delta}(\tilde{\boldsymbol{e}}_i\boldsymbol{a})$ can be found in [10,14]. Now, recalling Eq. (29) it is possible to rewrite the discrete form of Eq. (72) as:

$$\boldsymbol{a}\cdot\Delta\delta\boldsymbol{e}_i \cong \delta\hat{\boldsymbol{\theta}}^{T}\left[\sum_{j=1}^{nn} N_j\left[\boldsymbol{\Xi}\left(\boldsymbol{a},\hat{\boldsymbol{e}}_i^{j}\right) + \boldsymbol{T}_{\Delta}\tilde{\boldsymbol{a}}\tilde{\hat{\boldsymbol{e}}}_i^{j}\boldsymbol{T}_{\Delta}^{T}\right]\right]\Delta\hat{\boldsymbol{\theta}}, \tag{74}$$

where

$$\boldsymbol{\Xi}\left(\boldsymbol{a},\hat{\boldsymbol{e}}_i^{j}\right) = D[\boldsymbol{T}_{\Delta}(\tilde{\boldsymbol{e}}_i\boldsymbol{a})]\cdot\Delta\boldsymbol{\theta}. \tag{75}$$

In the same form, the expression for the second variation of the director's derivatives can be found in its discrete form by making use of Eq. (70):

$$\boldsymbol{a}\cdot\Delta\delta\boldsymbol{e}_i' = \delta\hat{\boldsymbol{\theta}}^{T}\left[\sum_{j=1}^{nn} N_j'\left[\boldsymbol{\Xi}\left(\boldsymbol{a},\hat{\boldsymbol{e}}_i^{j}\right) + \boldsymbol{T}_{\Delta}\tilde{\boldsymbol{a}}\tilde{\hat{\boldsymbol{e}}}_i^{j}\boldsymbol{T}_{\Delta}^{T}\right]\right]\Delta\hat{\boldsymbol{\theta}}. \tag{76}$$

5.3. Discrete virtual strains

Having derived the expressions for the discrete virtual directors, its derivatives and its corresponding linearization, it is now possi-

ble to find a discrete expression for the discrete virtual generalized strain and its linearization.

We can relate the intermediate vector $\delta\boldsymbol{\varphi}$ to the kinematic vector $\delta\boldsymbol{\phi} = \left[\begin{array}{cc}\delta\hat{\boldsymbol{u}}_{0j} & \delta\hat{\boldsymbol{\theta}}_j\end{array}\right]^T$ by means of a nodal matrix $\mathbb{B}$ as:

$$\delta\boldsymbol{\varphi} \cong \sum_{j=1}^{nn} \mathbb{B}_j \delta\hat{\boldsymbol{\phi}}_j, \tag{77}$$

where

$$\mathbb{B}_j = \begin{bmatrix} \boldsymbol{N}_j' & \boldsymbol{0} \\ \boldsymbol{0} & N_j \boldsymbol{T}_{\Delta j}^T \\ \boldsymbol{0} & N_j \tilde{\boldsymbol{e}}_2^{jT} \boldsymbol{T}_{\Delta j}^T \\ \boldsymbol{0} & N_j \tilde{\boldsymbol{e}}_3^{jT} \boldsymbol{T}_{\Delta j}^T \\ \boldsymbol{0} & N_j' \tilde{\boldsymbol{e}}_2^{jT} \boldsymbol{T}_{\Delta j}^T \\ \boldsymbol{0} & N_j' \tilde{\boldsymbol{e}}_3^{jT} \boldsymbol{T}_{\Delta j}^T \end{bmatrix}, \tag{78}$$

where $\tilde{}$ indicates the skew symmetric matrix of a vector and $\wedge$ indicates a nodal variable. Thus $\tilde{\boldsymbol{e}}_j^i$ is a skew director in the direction j of the node i and $\boldsymbol{T}_{\Delta j}^T$ is the transpose of the incremental tangential transformation at the node j. Henceforth summation over index j will be implicitly defined, so we will omit the summation symbol and the node index j.

Finally, recalling Eq. (36) we can write the virtual generalized strains as:

$$\delta\boldsymbol{\varepsilon} \cong \mathbb{H}\mathbb{B}\delta\hat{\boldsymbol{\phi}}. \tag{79}$$

The discrete form of the incremental virtual strains, i.e. $\Delta\delta\boldsymbol{\varepsilon}$, is more difficult to obtain. Using the structure of the geometric stiffness operator of Eq. (50) we can obtain a matrix $\mathbb{G}$ as to satisfy the equality $\Delta\delta\boldsymbol{\varepsilon}^T\boldsymbol{S} = \delta\boldsymbol{\varphi}^T\mathbb{G}\Delta\boldsymbol{\varphi}$, a lengthy manipulation gives:

$$\mathbb{G} = \begin{bmatrix} \overline{S}_1 & \boldsymbol{0} & \overline{Q}_2 & \overline{Q}_3 & \overline{M}_3 & \overline{M}_2 \\ & \boldsymbol{A} & \boldsymbol{0} & \boldsymbol{0} & \boldsymbol{0} & \boldsymbol{0} \\ & & \boldsymbol{0} & \boldsymbol{0} & \boldsymbol{0} & \boldsymbol{0} \\ & & & \boldsymbol{0} & \overline{M}_1 & \boldsymbol{0} \\ & Sym & & & 2\overline{P}_2 & \overline{P}_{23} \\ & & & & & 2\overline{P}_3 \end{bmatrix}, \tag{80}$$

where the term $\boldsymbol{A}$ is equivalent to that of the Total Lagrangian Formulation [13], except that the total tangential transformation must be replaces by the incremental tangential transformation.

5.4. The tangent stiffness matrix

The derivation of the tangent stiffness matrix is similar to that of the Total Lagrangian formulation, so we present it here briefly. Introducing Eq. (77) into Eq. (49) we can obtain the discrete form of the material virtual work as:

$$D_1\delta W_i(\hat{\boldsymbol{\phi}}, \delta\hat{\boldsymbol{\phi}}) \cdot \Delta\hat{\boldsymbol{\phi}} = \int_\ell (\mathbb{B}\delta\hat{\boldsymbol{\phi}})^T \mathbb{H}^T \mathbb{D}\mathbb{H}(\mathbb{B}\Delta\hat{\boldsymbol{\phi}}) dx. \tag{81}$$

Then, the element material stiffness matrix is:

$$\boldsymbol{k}_M = \int_\ell \mathbb{B}^T\mathbb{H}^T\mathbb{D}\mathbb{H}\mathbb{B} dx. \tag{82}$$

Proceeding in a similar way, we use Eqs. (80) and (50) to obtain the discrete geometric stiffness terms as:

$$D_2\delta W_i(\hat{\boldsymbol{\phi}}, \delta\hat{\boldsymbol{\phi}}) \cdot \Delta\hat{\boldsymbol{\phi}} = \int_\ell (\mathbb{B}\delta\hat{\boldsymbol{\phi}})^T \mathbb{G}(\mathbb{B}\Delta\hat{\boldsymbol{\phi}}) dx. \tag{83}$$

Therefore, the element geometric stiffness matrix becomes:

$$\boldsymbol{k}_G = \int_\ell \mathbb{B}^T\mathbb{G}\mathbb{B} dx. \tag{84}$$

Following the standard steps of the finite element method, the element and global tangent stiffness matrices are:

$$\begin{aligned} \boldsymbol{k}_T &= \int_\ell \mathbb{B}^T(\mathbb{H}^T\mathbb{D}\mathbb{H} + \mathbb{G})\mathbb{B} dx, \\ \mathbb{K} &= \sum_{e=1}^{els} \boldsymbol{k}_T, \end{aligned} \tag{85}$$

where the summation operator is used to represent the finite element assembly process.

5.5. The tangent mass matrix

Using linear interpolation for the acceleration field, i.e. $\ddot{\boldsymbol{\phi}} = \sum_{j=1}^{nn} \mathbb{N}_j \ddot{\hat{\boldsymbol{\phi}}}_n$, we can obtain the discrete version of the mass matrix of the Eq. (56). First, the discrete version of the linearized virtual work of the acceleration forces is written as:

$$D\delta W_a(\boldsymbol{\phi}, \delta\boldsymbol{\phi}) \cdot [\Delta(\boldsymbol{\phi}, \dot{\boldsymbol{\phi}}, \ddot{\boldsymbol{\phi}})] \cong \int_l \delta\hat{\boldsymbol{\phi}}^T \mathbb{N}^T\mathbb{M}\mathbb{N}\Delta\ddot{\hat{\boldsymbol{\phi}}} dx, \tag{86}$$

where $\wedge$ indicates nodal values and we have defined $\mathbb{N} = \sum_{j=1}^{nn} \mathbb{N}_j$ and

$$\delta\boldsymbol{\phi} \cong \sum_{j=1}^{nn} \mathbb{N}_j \delta\hat{\boldsymbol{\phi}}^j. \tag{87}$$

Implicitly assuming summation over index j we can write the discrete form for the tangent mass matrix (56) as:

$$\boldsymbol{M} = \int_l \mathbb{N}^T\mathbb{M}\mathbb{N} dx. \tag{88}$$

6. Multibody dynamics

6.1. Equations of motion of the constrained system

The formulation of the dynamic behavior of multibody systems gives a set of differential-algebraic system of equations if Lagrange multipliers are used to impose the constraints [45]. In the present work, the numerical solution of the constrained algebraic problem is found through the augmented Lagrangian method.

The equations of motion of the multibody system are:

$$\begin{cases} \boldsymbol{M}\ddot{\boldsymbol{\phi}} + \boldsymbol{B}^T(p\boldsymbol{\Phi} + k\boldsymbol{\lambda}) = \boldsymbol{g}(\boldsymbol{\phi}, \dot{\boldsymbol{\phi}}, t) \\ k\boldsymbol{\Phi}(\boldsymbol{\phi}, t) = \boldsymbol{0}, \end{cases} \tag{89}$$

where $\boldsymbol{B}^T$ is the constraints gradient matrix, $\boldsymbol{\Phi}$ is the constraints vector, $\boldsymbol{\lambda}$ is the Lagrange multipliers vector and $\boldsymbol{g}$ is the apparent forces vector (sum of internal, external and complementary inertia forces). Also, p and k are the penalty and scaling factors.

The linearized discrete equations of motion are obtained using Eqs. (5) and (8) as:

$$\begin{bmatrix} \mathbb{M} & \boldsymbol{0} \\ \boldsymbol{0} & \boldsymbol{0} \end{bmatrix} \begin{bmatrix} \Delta\ddot{\hat{\boldsymbol{\phi}}} \\ \Delta\boldsymbol{\lambda} \end{bmatrix} + \begin{bmatrix} \mathbb{K} + p\boldsymbol{B}^T\boldsymbol{B} & k\boldsymbol{B}^T \\ k\boldsymbol{B} & \boldsymbol{0} \end{bmatrix} \begin{bmatrix} \Delta\hat{\boldsymbol{\phi}} \\ \Delta\boldsymbol{\lambda} \end{bmatrix} = \begin{bmatrix} \boldsymbol{r} \\ -\boldsymbol{\Phi} \end{bmatrix}, \tag{90}$$

where r is the vector of residual forces:

$$\boldsymbol{r} = \boldsymbol{g}(\boldsymbol{\phi}, \ddot{\boldsymbol{\phi}}, t) - \mathbb{M}\ddot{\hat{\boldsymbol{\phi}}} - \boldsymbol{B}^T(p\boldsymbol{\Phi} + k\boldsymbol{\lambda}). \tag{91}$$

It is interesting note that we have neglected dependence of inertia forces with the configuration, which is consistent with the presented derivation of the inertial virtual work. Also, since the penalty factor was chosen to be sufficiently large, we assumed that the effect of the geometric stiffness associated to the Lagrange multipliers is negligible compared to the effect of the penalty term, i.e. $p\boldsymbol{B}^T\boldsymbol{B} \gg \partial_{\boldsymbol{\phi}}(k\boldsymbol{B}^T\boldsymbol{\lambda})$.

6.2. The viscous hinge joint

In a horizontal axis wind turbine the mechanism that connects the tower and the rotor can be modeled as a viscous hinge joint; we present in what follows the formulation of this typical joint in the framework of the present formulation. Extension of the formulation to other joints is straightforward.

The formulation of joints is based on kinematic relations between the configuration variables of two nodes. Often, the treatment of rotation kinematic constraints is aided by the definition of nodal triads that are not part of the beam finite element formulation. In the present formulation, the treatment of rotational constraints is greatly simplified by that fact that nodal triads are part of the finite element model, and thus no additional triad definitions are needed.

Following the idea of Cardona et al. [19], each joint will be formulated as an element. Hence, an element stiffness matrix and an element internal force vector is provided by the joint formulation and assembled into the global system in a conventional manner and the Lagrange multipliers associated with the imposed constraints are treated as additional degrees of freedom.

The hinge imposes three vectorial constraints between two nodes, a displacement vector constraint and two director constraints. We express them as:

$$\boldsymbol{\Phi} = \begin{bmatrix} \boldsymbol{u}_B - \boldsymbol{u}_A \\ \boldsymbol{e}_1^A \cdot \boldsymbol{e}_2^B \\ \boldsymbol{e}_1^A \cdot \boldsymbol{e}_3^B \end{bmatrix} = 0. \tag{92}$$

The variation of the constraints give:

$$\delta\boldsymbol{\Phi} = \begin{bmatrix} \delta\boldsymbol{u}_B - \delta\boldsymbol{u}_A \\ \delta\boldsymbol{e}_1^A \cdot \boldsymbol{e}_2^B + \boldsymbol{e}_1^A \cdot \delta\boldsymbol{e}_2^B \\ \delta\boldsymbol{e}_1^A \cdot \boldsymbol{e}_3^B + \boldsymbol{e}_1^A \cdot \delta\boldsymbol{e}_3^B \end{bmatrix} = \begin{bmatrix} \delta\boldsymbol{u}_B - \delta\boldsymbol{u}_A \\ (\delta\tilde{\boldsymbol{w}}_A\boldsymbol{e}_1^A) \cdot \boldsymbol{e}_2^B + \boldsymbol{e}_1^A \cdot (\delta\tilde{\boldsymbol{w}}_B\boldsymbol{e}_2^B) \\ (\delta\tilde{\boldsymbol{w}}_A\boldsymbol{e}_1^A) \cdot \boldsymbol{e}_3^B + \boldsymbol{e}_1^A \cdot (\delta\tilde{\boldsymbol{w}}_B\boldsymbol{e}_3^B) \end{bmatrix}. \tag{93}$$

Reordering some terms and invoking Eq. (29) we can re-write the last expression as:

$$\delta\boldsymbol{\Phi} = \boldsymbol{B}\delta\hat{\boldsymbol{\phi}}, \quad \text{where} \quad \boldsymbol{B} = \begin{bmatrix} -\boldsymbol{I} & \boldsymbol{0} & \boldsymbol{I} & \boldsymbol{0} \\ \boldsymbol{0} & (\tilde{\boldsymbol{e}}_1^A\boldsymbol{e}_2^B)^T\boldsymbol{T}_1^T & \boldsymbol{0} & (\tilde{\boldsymbol{e}}_2^B\boldsymbol{e}_1^A)^T\boldsymbol{T}_2^T \\ \boldsymbol{0} & (\tilde{\boldsymbol{e}}_1^A\boldsymbol{e}_3^B)^T\boldsymbol{T}_1^T & \boldsymbol{0} & (\tilde{\boldsymbol{e}}_3^B\boldsymbol{e}_1^A)^T\boldsymbol{T}_2^T \end{bmatrix}. \tag{94}$$

In the above expression, $\boldsymbol{B}$ is the 5×12 constraints gradient matrix. As it can be seen, the expression of the constraints gradient matrix is very simple and does not contain the rotation tensor.

Now, the discrete equation of motion for a rigid and massless hinge element can be written as:

$$\begin{bmatrix} p\boldsymbol{B}^T\boldsymbol{B} & k\boldsymbol{B}^T \\ k\boldsymbol{B} & \boldsymbol{0} \end{bmatrix} \begin{bmatrix} \Delta\hat{\boldsymbol{\phi}} \\ \Delta\boldsymbol{\lambda} \end{bmatrix} = \begin{bmatrix} -\boldsymbol{B}^T(p\boldsymbol{\Phi} + k\boldsymbol{\lambda}) \\ -\boldsymbol{\Phi} \end{bmatrix}. \tag{95}$$

Both the pseudo stiffness matrix and the pseudo internal forces vector are assembled into the global system in a conventional fashion.

The derivation of the viscous forces requires some algebraic manipulation. The rotational relation between the master and slave nodes of the hinge can be expressed as:

$$\boldsymbol{\Lambda}_s = \boldsymbol{\Lambda}_m\boldsymbol{\Lambda}_j, \tag{96}$$

where $\boldsymbol{\Lambda}_s$, $\boldsymbol{\Lambda}_m$ and $\boldsymbol{\Lambda}_j$ are the rotation tensor of the slave node, the rotation tensor of the master node and the joint rotation tensor. The joint rotation tensor can obtained through the exponential map of the joint rotation vector:

$$\boldsymbol{\theta}_j = \boldsymbol{\theta}_s - \boldsymbol{\theta}_m, \tag{97}$$

where $\boldsymbol{\theta}_s$ and $\boldsymbol{\theta}_m$ are the slave node and the master node rotation vector, respectively. Note that addition can be done since both vectors belong to the same tangent space, i.e. $\boldsymbol{T}^m_{\boldsymbol{\Lambda}_R}$, being $\boldsymbol{\Lambda}_R$ the reference rotation tensor.

The viscous moment originated in the joint can be seen as an entity of T^m_Λ because of its proportionality with the material angular velocity, this is:

$$\overline{\boldsymbol{M}}_v = c_v\boldsymbol{\Omega}_j, \tag{98}$$

being $\boldsymbol{\Omega}_j$ the material angular velocity of the joint, which can be written as:

$$\boldsymbol{\Omega}_j = T_j(\dot{\boldsymbol{\theta}}_s - \dot{\boldsymbol{\theta}}_m), \tag{99}$$

where we have exploited the relation $\dot{\boldsymbol{\theta}}_j = \dot{\boldsymbol{\theta}}_s - \dot{\boldsymbol{\theta}}_m$.

According to a material description, the virtual work of the dissipative torque is:

$$dW_v = \delta\boldsymbol{\Theta}_j \cdot \overline{\boldsymbol{M}}_v = \delta\boldsymbol{\Theta}_j \cdot c_v\boldsymbol{\Omega}_j. \tag{100}$$

The expression of the material spin of the joint, i.e. $\delta\,\boldsymbol{\Theta}_j$, can be obtained calculating the variation of Eq. (96), this is:

$$\begin{aligned} &\delta\boldsymbol{\Lambda}_s = \delta\boldsymbol{\Lambda}_m\boldsymbol{\Lambda}_j + \boldsymbol{\Lambda}_m\delta\boldsymbol{\Lambda}_j, \\ &\boldsymbol{\Lambda}_s\delta\widetilde{\boldsymbol{\Theta}}_s = \boldsymbol{\Lambda}_m\delta\widetilde{\boldsymbol{\Theta}}_m\boldsymbol{\Lambda}_j + \boldsymbol{\Lambda}_m\boldsymbol{\Lambda}_j\delta\widetilde{\boldsymbol{\Theta}}_j. \end{aligned} \tag{101}$$

Using some algebra we can obtain:

$$\delta\boldsymbol{\Theta}_j = \delta\boldsymbol{\Theta}_s - \boldsymbol{\Lambda}_j^T\delta\boldsymbol{\Theta}_m. \tag{102}$$

Then the virtual work of the dissipative moments reads:

$$dW_v = \left(\delta\boldsymbol{\Theta}_s - \boldsymbol{\Lambda}_j^T\delta\boldsymbol{\Theta}_m\right) \cdot [c_v\boldsymbol{T}_j(\dot{\boldsymbol{\theta}}_s - \dot{\boldsymbol{\theta}}_m)]. \tag{103}$$

In matrix form it can be written as:

$$dW_v = \delta\boldsymbol{\theta}^T\mathbb{C}_v\dot{\boldsymbol{\theta}}$$
$$\mathbb{C}_v = c_v\begin{bmatrix} \boldsymbol{T}_s\boldsymbol{T}_j & -\boldsymbol{T}_s\boldsymbol{T}_j \\ -\boldsymbol{\Lambda}_j^T\boldsymbol{T}_m\boldsymbol{T}_j & \boldsymbol{\Lambda}_j^T\boldsymbol{T}_m\boldsymbol{T}_j \end{bmatrix}, \quad \delta\boldsymbol{\theta} = \begin{bmatrix} \delta\boldsymbol{\theta}_s \\ \delta\boldsymbol{\theta}_m \end{bmatrix}, \quad \dot{\boldsymbol{\theta}} = \begin{bmatrix} \dot{\boldsymbol{\theta}}_s \\ \dot{\boldsymbol{\theta}}_m \end{bmatrix}. \tag{104}$$

From the above development we can finally obtain the viscous nodal moment vector as:

$$\overline{\overline{\boldsymbol{M}}}_v = \mathbb{C}_v\dot{\boldsymbol{\theta}}. \tag{105}$$

The Updated Lagrangian version of the matrix $\mathbb{C}_v$ is simply:

$$\mathbb{C}_v = c_v\begin{bmatrix} \boldsymbol{T}_{\Delta s}\boldsymbol{T}_{\Delta j} & \boldsymbol{T}_{\Delta s}(-\boldsymbol{T}_{\Delta j}) \\ -(\boldsymbol{\Lambda}_{Rj}\boldsymbol{\Lambda}_{\Delta j})^T\boldsymbol{T}_m\boldsymbol{T}_j & (\boldsymbol{\Lambda}_{Rj}\boldsymbol{\Lambda}_{\Delta j})^T\boldsymbol{T}_{\Delta m}\boldsymbol{T}_{\Delta j} \end{bmatrix}, \tag{106}$$

where the subscript Δ indicates an incremental matrix and the subscript R indicates reference; thus, $\boldsymbol{\Lambda}_{Rj}$ and $\boldsymbol{\Lambda}_{\Delta j}$ are the reference and incremental rotation matrices of the joint respectively.

7. Application

7.1. A simple two body test

In order to evaluate the performance of the multibody implementation of the present finite element, we set a double pendulum beam configuration made of EGlass-Epoxy that falls under the effect of gravity. The pendulum has a square cross-section with $b = 0.1$, $h = 0.1$, $e = 0.01$, laminated in a {45, −45, −45, 45} configuration, see Fig. 4. The material properties of the composite layers are given in Table 1; E_{xx} is the Young modulus in the axial direction, E_{ss} is the Young modulus in the tangential direction, G_{xs} is the in-plane shear modulus, G_{xn} is the transverse shear modulus and ν_{xs} is the in-plane Poisson modulus. Note that x is the longitudinal axis of the pendulum.

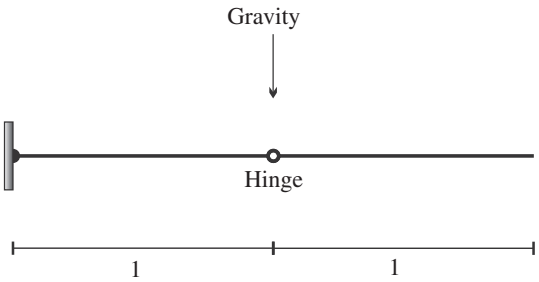

Fig. 4. Bi-pendulum configuration.

Table 1
Material properties of EGlass–Epoxy.

E_{xx}	E_{ss}	G_{xs}	G_{xn}	ν_{xs}	ρ
45.0×10^9	12.0×10^9	5.5×10^9	5.5×10^9	0.3	2000

We compare the proposed pendulum against an Abaqus 3D shell model, the Fig. 5 presents the evolution of the tip vertical displacements in time.

It can be seen from Fig. 5 that the displacements obtained with the present finite element exactly match those obtained with the Abaqus Shell model; the same agreement is obtained in velocities and accelerations. It must be noted that since the double pendulum quickly adopts a chaotic behavior, the correlation suddenly ends after a not very long period of time. Although both formulations are written in different platforms and computational cost comparisons may be not accurate, a glance at time consumptions shows that performing 1000 time steps takes Abaqus 1092 s, while the proposed finite element Matlab implementation takes only 240 s.

7.2. Application to wind turbine modeling

In the following we present the results of the application of the present finite element to the simulation of a modern wind turbine design. This wind turbine experiment displacements and rotations in the nonlinear range, where the present finite element should behave efficiently.

The wind turbine is a 13.2 MW machine, its configuration and design parameters were obtained from [47]. The machine has three 100 m long blades and an all fiberglass material mapping, see Fig. 6 (dimension are in meters).

The multibody wind turbine model consist of 66 finite elements: 51 beam finite elements were used to discretize the blades (17 elements per blade), 2 rigid and 2 mass finite elements were used to model the nacelle, a viscous joint element was used to model the tower-rotor interaction and 10 beam elements were used for the tower. Excepting for the joint and the nacelle elements, all the finite elements assume a composite material mapping as specified in [47].

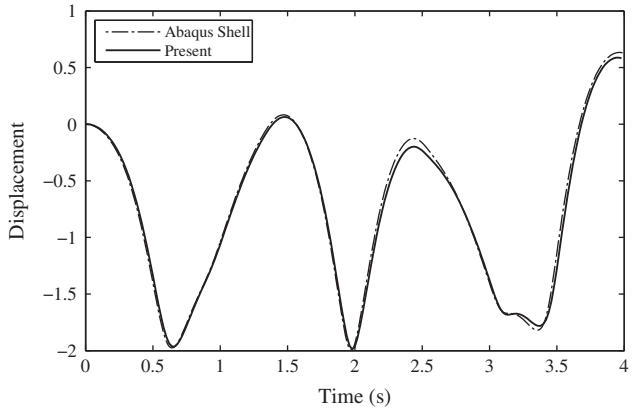

Fig. 5. Tip displacements of the composite bi-pendulum.

The aerodynamic forces were obtained by a BEM based aeroelastic formulation that is consistent with the finite kinematic hypothesis; this formulation will be presented in a future work. It must be noted that most of the tests were conducted without considering the effect of structural damping, mainly because the traditional damping models that assume that damping forces are a function of the configuration velocities are not consistent with geometrically exact concept. However, in order to have a quick picture of the effects of structural damping in the response of the system, we have briefly analyzed at the end of this section a simplified solution of the inclusion of structural damping.

7.3. Wind turbine start

Firstly, we test the behavior of the multibody formulation when modeling the wind turbine during its start process. This is a very important test since the induced vibrations in the wind turbine reach its maximum during the start, and thus not only the time integration algorithm must deal with fast transient conditions but also the structural formulation must deal with high strains and stresses.

There are several ways to bring the wind turbine multibody model into motion, e.g.: impose a velocity field in the rotor, impose a torque in the hinge joint, impose a tangential force in the blades, etc. The imposition of the velocity field requires a special programming routine for assigning to every degree of freedom the corresponding velocity (which is quite complex for the rotations). The imposition of a hinge torque is very simple, but convergence is difficult to obtain when it is desired to get a high angular acceleration. Finally, using a tangential force to induce the motion is very simple since finite rotations do not play a role in the imposition algorithm and also there are no convergence inconveniences.

Considering the comments above, the test starts with the imposition of a tangential force in the blades lasting 2 s. Then the force is set to zero and a wind blowing at 13 m/s is imposed; the wind continues blowing for 18 s. We chose to make the starting process very fast since it makes the system to oscillate quickly and then the multibody formulation can be tested.

The Fig. 7 presents the first 20 s of the evolution of the flapping acceleration at the three blade tips. As it can be seen, the high frequency vibrations induced by the starting force are quickly damped out by the aerodynamic damping (note that no structural damping was considered). On the contrary, the blade free vibrations that occur after retiring the force are not damped by the aerodynamic forces.

The same behavior can be observed on the root flap-wise and lag-wise moments, see Figs. 7 and 8. It is important to note that the present finite element naturally gives the flap-wise and lag-wise moments as a result, i.e. it is not necessary to perform any force or moment projections. This is because the generalized forces (and moments) are defined in the element coordinate system, which has local triads oriented normal and parallel to the chord, i.e in the flap-wise and lag-wise directions.

7.4. Normal power production

Now we present the results obtained for the normal operating condition of the wind turbine; according to the IEC Standard, this condition is generated by a 11.3 m/s wind velocity. The test is con-

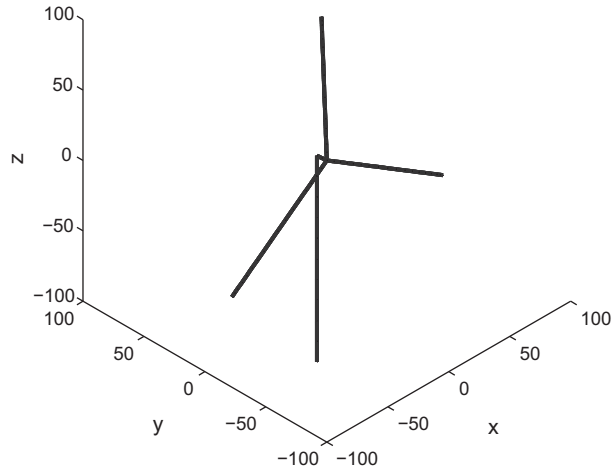

Fig. 6. Wind turbine geometry.

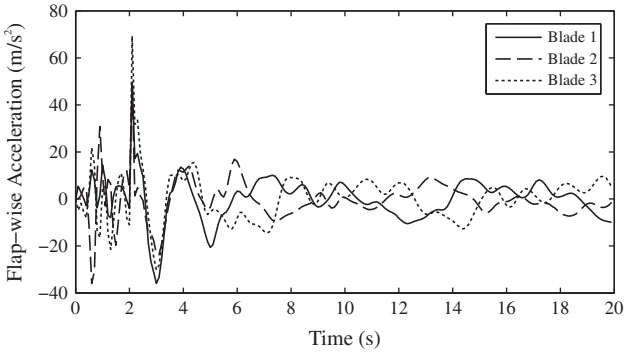

Fig. 7. Blade tip accelerations during the wind turbine start.

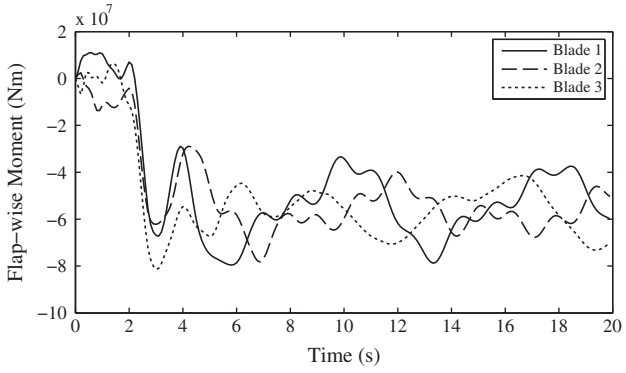

Fig. 8. Flap-wise root moments during the wind turbine start.

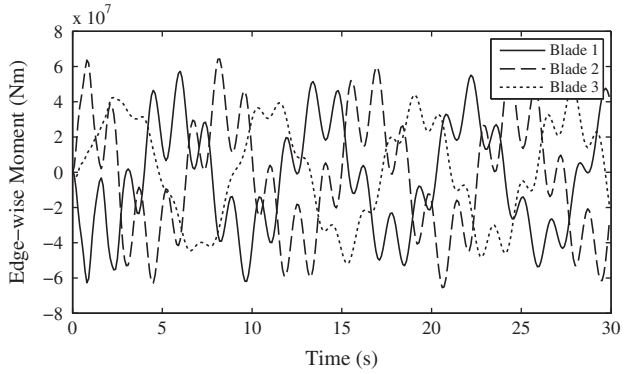

Fig. 9. Lag-wise root moments during the wind turbine start.

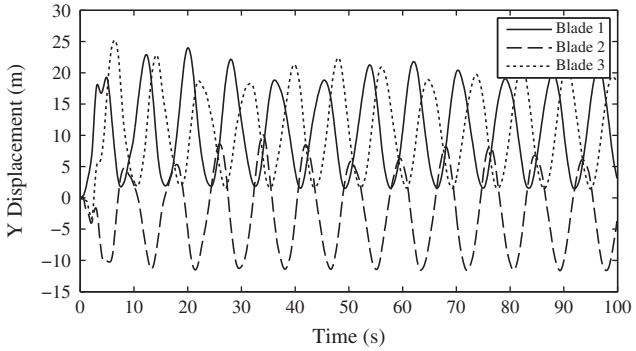

Fig. 10. Y displacements at blades tip.

ducted during 100 s, what is enough to get the steady state response of the wind turbine (see Fig. 9).

The Fig. 10 shows the evolution of the tip displacements at the three blades. To understand the time history of displacement it must be noted that the wind turbine rotor is spatially rotated in two axed by the pre-cone and tilt angles, 5 and 2.5 degrees respectively. As it can be seen, the displacement time history is consistent with the wind turbine geometry. However it must be stressed the fact that in the present formulation the displacements and rotations of the bodies has a "total" meaning; thus it is not possible to directly obtain from the time histories of the kinematic variables the magnitudes of the displacements and rotations that is associated to the deflection of a certain component of the multibody system. Of course, this drawback can easily be overcome by different methods, as for example adding tracking references frames.

Fig. 11 show the evolution of the flap-wise root moments for the three blades during the whole test. The bending moments in the blades give consistent results when comparing the blades to each other. Also, the magnitudes of the moments agree with those obtained by means of the linear beam multibody model used in [47], which predicts a flap-wise moment of approximately 5000 KNm.

The Fig. 12 shows the evolution of the angle of attack, measured in degrees, for three different positions of one of the blades. It can also be seen that angle of attack oscillates during the whole test, this oscillation is generated by different sources: (i) by the flexural-torsional geometrical and constitutive coupling in the blade, (ii) by the cone shape of the plane of rotation and (iii) by the aerodynamic moment. In a future work the incidence of this sources in the magnitude of the effective angle of attack will be analyzed in detail. Note that the angle of attack is near 80 degrees at the start of the test because at this time the tangential velocity of the blade

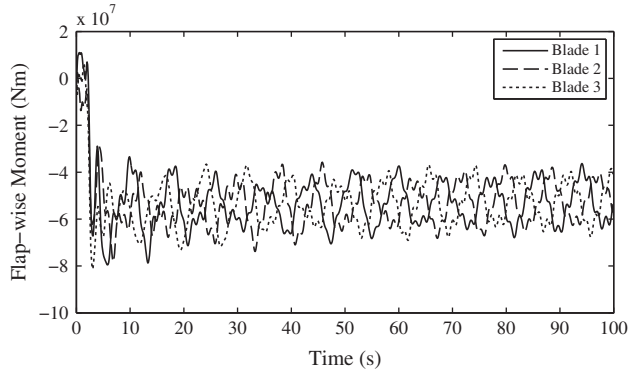

Fig. 11. Flap-wise moments at blade roots.

is zero and then the local blade velocity is a result of the wind speed only.

7.5. Simplified damping modeling

As it was stated before, the vibration of the blades is damped by both the structural and the aerodynamic damping. However, it is very important to note that in the present formulation the typical techniques for applying the structural damping cannot always be applied consistently without damping the rigid body motion; this is the case of Rayleigh damping. This is because the velocity vector has a total meaning, which implies that it is not possible to know what portion of the velocity of a point associated to a certain deflection and what portion is associated to a rigid body motion. Therefore, if one assumes that the damping forces are a function of the configuration velocities, then these forces commonly contain a fictitious component associated to the rigid body motion. A common procedure for modeling damping in multibody dynamics is to use stiffness proportional damping, in which the fact that the rigid body velocity vector lies in the nullspace of the stiffness matrix ensures that there the mentioned rigid body damping forces do not exist. Although stiffness proportional damping damps excessively the higher frequencies and do not provides low frequency damping, it is a very attractive approach because of its simplicity. This is the approach the we used in the present example.

The Figs. 12 and 13 show the response of the multibody wind turbine model during the start. As it can be seen, the effect of the structural damping on the blade vibration is responsible for damping the free vibration modes.

Considering the results presented above and the fact that a consistent formulation for the structural damping as configuration velocities proportional form is not convenient in the present context, it is undoubtedly necessary to derive an alternative formulation for the structural damping; probably, to consider the damping forces as a function of the strain rate could be effective.

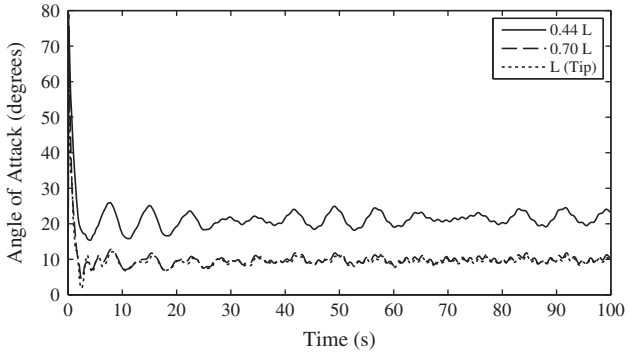

Fig. 12. Angle of attack history.

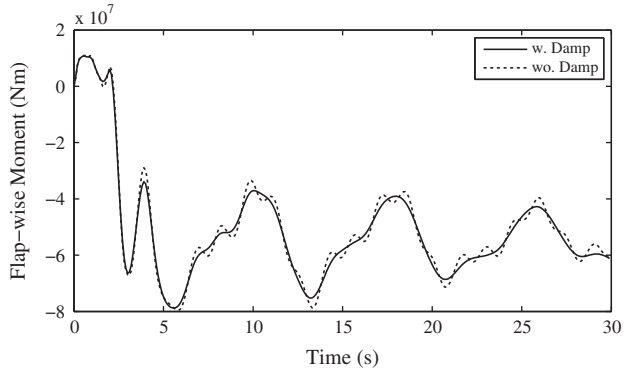

Fig. 13. Structural damping effect on the flap-wise root moment.

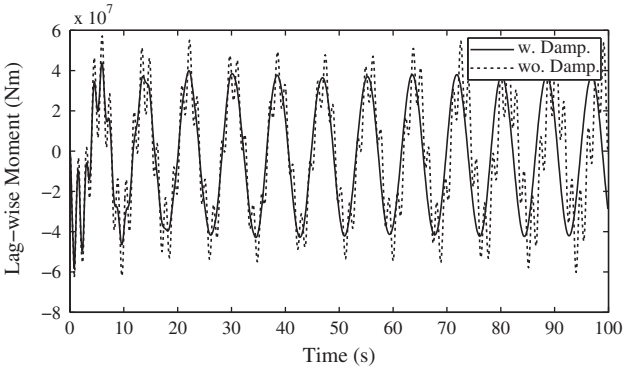

Fig. 14. Structural damping effect on the lag-wise root moment.

7.6. Normal wind turbine operation with transient gust

We analyze in the present example the behavior of the multibody wind turbine model in a high deformation scenario originated by an operating gust in the absence of a control system for the generator brake. In this case, the wind blows with a mean value of 11.3 m/s and a gust of 25 m/s is imposed linearly from 20 to 40 s (see Fig. 14).

The Fig. 15 shows the time history of the flap-wise moments in the blade roots and the Fig. 16 shows the deformed shape of the

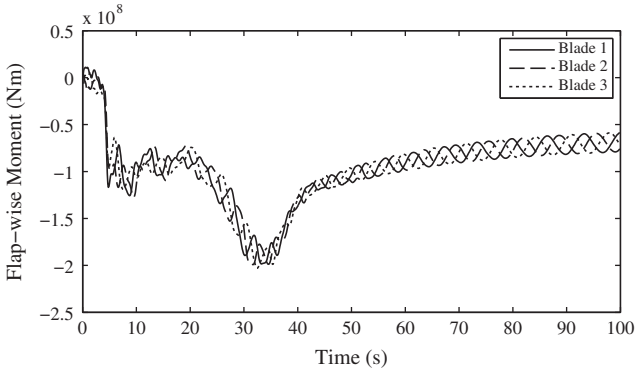

Fig. 15. Flap-wise root moments during normal gust.

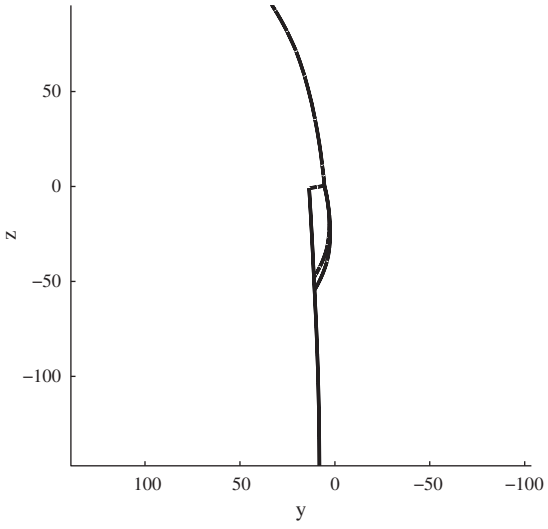

Fig. 16. Deformed shape during normal gust.

wind turbine for an instant near the maximum deflection configuration. The proposed formulation results to be very stable still in this high deformation scenario.

8. Conclusions

An Updated Lagrangian geometrically exact composite beam element for multibody applications has been presented. In the proposed formulation the virtual work equations was written as a function of generalized strains, which are parametrized in terms of the director field and its derivatives.

The theoretical background of the formulation of the cross-sectional properties was briefly presented. Details about the application of the classical lamination theory to the obtention of the cross-sectional stiffness of complex cross-sections were also presented.

Different characteristic aspects of the multibody problem, such as the handling of finite rotations and the formulation of joints have also been addressed; it was given special attention to the modeling details that arise in wind turbine applications. The formulation of a viscous hinge joint was developed. The joint permits to represent the interaction between the tower and the rotor considering the torque given to the generator as a dissipative moment.

Several examples of the application of the proposed formulation to the case of a large wind turbine were presented. The tests showed that the formulation is very stable and effective still under conditions of large deformation.

Acknowledgements

The authors wish to acknowledge the supports from Secretaría de Ciencia y Tecnología of Universidad Tecnológica Nacional and CONICET.

References

[1] Simo JC. A finite strain beam formulation. The three-dimensional dynamic problem. Part I. Computer Methods in Applied Mechanics and Engineering 1985;49:55–70.
[2] Cardona A, Geradin M. A beam finite element non-linear theory with finite rotations. International Journal for Numerical Methods in Engineering 1988;26:2403–38.
[3] Ibrahimbegovic A. On finite element implementation of geometrically nonlinear Reissner's beam theory: three-dimensional curved beam elements. Computer Methods in Applied Mechanics and Engineering 1995;122:11–26.
[4] F. Armero, I. Romero, On the objective and conserving integration of geometrically exact rod models, in: Proc. Trends in Computational Structural Mechanics, CIMNE, Barcelona, Spain, 2001.
[5] Betsch P, Steinmann P. Frame-indifferent beam finite elements based upon the geometrically exact beam theory. International Journal for Numerical Methods in Engineering 2002;54:1775–88.
[6] Crisfield MA. Non-Linear Finite Element Analysis of Solids and Structures: Advanced Topics. John Wiley & Sons, Inc.; 1997.
[7] Ibrahimbegovic A, Al Mikdad M. Finite rotations in dynamics of beams and implicit time-stepping schemes. International Journal for Numerical Methods in Engineering 1998;41:781–814.
[8] Ibrahimbegoviæ A, Frey F, Kožar I. Computational aspects of vector-like parametrization of three-dimensional finite rotations. International Journal for Numerical Methods in Engineering 1995;38:3653–73.
[9] Jelenic G, Crisfield MA. Geometrically exact 3D beam theory: implementation of a strain-invariant finite element for statics and dynamics. Computer Methods in Applied Mechanics and Engineering 1999;171:141–71.
[10] Ritto-Corrêa M, Camotim D. On the differentiation of the Rodrigues formula and its significance for the vector-like parameterization of Reissner-Simo beam theory. International Journal for Numerical Methods in Engineering 2002;55:1005–32.
[11] Saravia CM, Machado SP, Cortínez VH. A geometrically exact nonlinear finite element for composite closed section thin-walled beams. Computer and Structures 2011;89:2337–51.
[12] Simo JC, Vu-Quoc L. On the dynamics in space of rods undergoing large motions – a geometrically exact approach. Computer Methods in Applied Mechanics and Engineering 1988;66:125–61.
[13] Saravia MC, Machado SP, Cortínez VH. A consistent total Lagrangian finite element for composite closed section thin walled beams. Thin-Walled Structures 2012;52:102–16.
[14] Cesnik CES, Hodges DH. VABS: a new concept for composite rotor blade cross-sectional modeling. Journal of the American Helicopter Society 1997;42:27–38.
[15] Hodges DH. A mixed variational formulation based on exact intrinsic equations for dynamics of moving beams. International Journal of Solids and Structures 1990;26:1253–73.
[16] Yu W, Liao L, Hodges DH, Volovoi VV. Theory of initially twisted, composite, thin-walled beams. Thin-Walled Structures 2005;43:1296–311.
[17] Hodges DH. Nonlinear Composite Beam Theory. Virginia: American Institute of Aeronautics and Astronautics, Inc.; 2006.
[18] Hansen MOL, Sørensen JN, Voutsinas S, Sørensen N, Madsen HA. State of the art in wind turbine aerodynamics and aeroelasticity. Progress in Aerospace Sciences 2006;42:285–330.
[19] Cardona A, Geradin M, Doan DB. Rigid and flexible joint modelling in multibody dynamics using finite elements. Computer Methods in Applied Mechanics and Engineering 1991;89:395–418.
[20] Ibrahimbegovic A, Mamouri S. On rigid components and joint constraints in nonlinear dynamics of flexible multibody systems employing 3D geometrically exact beam model. Computer Methods in Applied Mechanics and Engineering 2000;188:805–31.
[21] Ibrahimbegovic A, Taylor RL, Lim H. Non-linear dynamics of flexible multibody systems. Computers & Structures 2003;81:1113–32.
[22] Hodges DH, Yu W. A rigorous, engineer-friendly approach for modelling realistic, composite rotor blades. Wind Energy 2007;10:179–93.
[23] Hansen MOL. Aerodynamics of Wind Turbines. London: Earthscan Publications Ltd.; 2008.
[24] Hau E. Wind Turbines. second ed. Berlin: Springer; 2006.
[25] Larsen JW, Nielsen SRK. Non-linear dynamics of wind turbine wings. International Journal of Non-Linear Mechanics 2006;41:629–43.
[26] Larsen JW, Nielsen SRK. Nonlinear parametric instability of wind turbine wings. Journal of Sound and Vibration 2007;299:64–82.
[27] M.L. Buhl, M. Andreas, A comparison of wind turbine aeroelastic codes used for certification, in: National Renewable Energy Laboratory, 2006.
[28] Wang J, Qin D, Lim TC. Dynamic analysis of horizontal axis wind turbine by thin-walled beam theory. Journal of Sound and Vibration 2010;329:3565–86.
[29] Zhao X, Maißer P, Wu J. A new multibody modelling methodology for wind turbine structures using a cardanic joint beam element. Renewable Energy 2007;32:532–46.
[30] M.L. Buhl, A.D. Wrigth, K.G. Pierce, Wind tubine design codes: a comparison of the structural response, in: NREL, 2000.
[31] C.L. Bottasso, Aeroelastic simulation of tilt-rotors using non-linear finite element multibody procedures, in: K.J. Bathe (Ed.), Second MIT Conference on Computational Fluid and Solid Mechanics, 2003, pp. 1267–1270.
[32] Bauchau OA, Bottasso CL, Nikishkov YG. Modeling rotorcraft dynamics with finite element multibody procedures. Mathematical and Computer Modelling 2001;33:1113–37.
[33] Bottasso C, Croce A, Savini B, Sirchi W, Trainelli L. Aero-servo-elastic modeling and control of wind turbines using finite-element multibody procedures. Multibody System Dynamics 2006;16:291–308.
[34] Dai JC, Hu YP, Liu DS, Long X. Aerodynamic loads calculation and analysis for large scale wind turbine based on combining BEM modified theory with dynamic stall model. Renewable Energy 2011;36:1095–104.
[35] Holm-Jørgensen K, Nielsen SRK. A component mode synthesis algorithm for multibody dynamics of wind turbines. Journal of Sound and Vibration 2009;326:753–67.
[36] T.J. Larsen, A.M. Hansen, T. Buhl, Aeroelastic effects of large blade deflections for wind turbines, in: D.U.o. Technology (Ed.), Proceeding of The Science of Making Torque from Wind, The Netherlands, 2004, pp. 238–246.
[37] Argyris J. An excursion into large rotations. Computer Methods in Applied Mechanics and Engineering 1982;32:85–155.
[38] Bonet J, Wood RD. Nonlinear Continuum Mechanics for Finite Element Analysis. Cambridge: Cambridge University Press; 1997.
[39] Barbero E. Introduction to Composite Material Design. London: Taylor and Francis; 2008.
[40] Jones RM. Mechanics of Composite Materials. London: Taylor & Francis; 1999.
[41] Washizu K. Variational Methods in Elasticity and Plasticity. Oxford: Pergamon Press; 1968.
[42] Zienkiewicz OC, Taylor RL. The Finite Element Method. Oxford: Buttherworth-Heinemann; 2000.
[43] Betsch P. On the parametrization of finite rotations in computational mechanics a classification of concepts with application to smooth shells. Computer Methods in Applied Mechanics and Engineering 1998;155:273–305.
[44] Mäkinen J. Total Lagrangian Reissner's geometrically exact beam element without singularities. International Journal for Numerical Methods in Engineering 2007;70:1009–48.
[45] Geradin M, Cardona A. Flexible Multibody Dynamics: A Finite Element Approach. Chichester: Wiley; 2001.
[46] C.M. Saravia, Dinámica Aeroelástica No Lineal de Aerogeneradores de Material Compuesto, Universidad Nacional del Sur, Bahía Blanca-Argentina, 2012.
[47] D.T. Griffith, T.D. Ashwill, The Sandia 100-m all-glass baseline wind turbine blade: SNL100-00, in: Sandia National Laboratories, 2011.